

An Analytical Study of PPP-RTK Corrections: Precision, Correlation and User-Impact

A. Khodabandeh · P.J.G. Teunissen

Received: date / Accepted: date

Abstract PPP-RTK extends the PPP-concept by providing single-receiver users, next to orbits and clocks, also information about the satellite phase and code biases, thus enabling single-receiver ambiguity resolution. It is the goal of the present contribution to provide an analytical study of the quality of the PPP-RTK corrections as well as of their impact on the user ambiguity resolution performance. We consider the geometry-free (GF) and the geometry-based (GB) network derived corrections, as well as the impact of network ambiguity resolution on these corrections. Next to the insight that is provided by the analytical solutions, the closed form expressions of the variance matrices also demonstrate how the corrections depend on network parameters such as number of epochs, number of stations, number of satellites, and number of frequencies. As a result we are able to describe in a qualitative sense how the user ambiguity resolution performance is driven by the data from the different network scenarios.

Keywords Global Navigation Satellite Systems (GNSS), Precise Point Positioning (PPP), Integer Ambiguity Resolution (IAR), PPP-RTK corrections, Geometry-Free (GF), Geometry-Based (GB), Ambiguity Dilution of Precision (ADOP)

A. Khodabandeh
GNSS Research Centre, Department of Spatial Sciences, Curtin University of Technology, Perth, Australia
E-mail: amir.khodabandeh@curtin.edu.au

P. J. G. Teunissen
GNSS Research Centre, Department of Spatial Sciences, Curtin University of Technology, Perth, Australia; Department of Geoscience and Remote Sensing, Delft University of Technology, Delft, The Netherlands
E-mail: p.teunissen@curtin.edu.au

1 Introduction

PPP-RTK is integer ambiguity resolution enabled precise point positioning (PPP) (Wubben et al, 2005; Mervart et al, 2008). It extends the PPP-concept (Heroux and Kouba, 1995; Zumberge et al, 1997) by providing single-receiver users, next to the orbits and clocks, also information about the satellite phase and code biases. This information, when properly provided, enables recovery of the integerness of the user-ambiguities, thus enabling single-receiver ambiguity resolution, thereby reducing convergence times as compared to that of PPP.

Several PPP-RTK methods have been formulated in recent years, see e.g., Wubben et al (2005); Laurichesse and Mercier (2007); Mervart et al (2008); Collins (2008); Ge et al (2008); Bertiger et al (2010); Teunissen et al (2010); Geng et al (2012); Loyer et al (2012); Geng and Bock (2013); Lannes and Prieur (2013); Banville et al (2014). For an overview and a critical comparison of these methods, see the review (Teunissen and Khodabandeh, 2015). As was demonstrated in (ibid), a careful interpretation of the estimable parameters involved is essential for obtaining a proper insight into the general mechanics of PPP-RTK. It is the goal of the present contribution to take this one step further by providing an analytical study of the multi-frequency PPP-RTK corrections themselves, thereby presenting a precision and correlation analysis that will enable us to demonstrate how the quality of these corrections, as well as their impact on the user parameters, are driven by the information content and adjustment of the external network.

PPP-RTK is founded on the idea of single-receiver integer ambiguity resolution (IAR). This idea, together with the estimability of the associated PPP-RTK corrections, is best described by starting with the single-

receiver user observation equations. Consider the user's antenna u tracking f -frequency GNSS data that are transmitted by a satellite s and a chosen pivot satellite p . The corresponding between-satellite single-difference (SD) observation equations read then (Teunissen and Kleusberg, 1998; Hofmann-Wellenhof et al, 2008)

$$\begin{aligned}\Delta\phi_{u,j}^{ps} &= g^{psT} \Delta x_u - \mu_j \iota_u^{ps} - dt^{ps} + \lambda_j (z_{u,j}^{ps} - \delta_{,j}^{ps}) \\ \Delta p_{u,j}^{ps} &= g^{psT} \Delta x_u + \mu_j \iota_u^{ps} - dt^{ps} - \tilde{d}_{,j}^{ps}\end{aligned}\quad (1)$$

where $\Delta\phi_{u,j}^{ps}$ and $\Delta p_{u,j}^{ps}$ denote the SD 'observed-minus-computed' phase and code observables on the frequency band f_j ($j = 1, \dots, f$), respectively. Here and in the following, the precise orbital corrections are assumed included in the 'observed-minus-computed' observables. The ν -vector Δx_u contains the user's position increments and/or the zenith tropospheric delay (ZTD). Parameter ν can take the values $\nu = 3$ (position-only model), $\nu = 1$ (ZTD-only model) or $\nu = 4$ (position-plus-ZTD model). Thus the ν -vector g^{ps} contains the SD receiver-satellite direction vector and/or the SD tropospheric mapping function. The (first-order) SD slant ionospheric delay, experienced on the first frequency, is denoted by ι_u^{ps} . Thus the frequency-dependent coefficients are defined as the ratio $\mu_j = (f_1^2/f_j^2)$. The SD integer ambiguity $z_{u,j}^{ps} \in \mathbb{Z}$ and the SD satellite phase bias $\delta_{,j}^{ps}$, both expressed in cycles, are linked to the phase observables through the wavelength λ_j . The SD satellite clocks are denoted by dt^{ps} , while the SD satellite code biases are denoted by $\tilde{d}_{,j}^{ps}$. Apart from $z_{u,j}^{ps}$ and $\delta_{,j}^{ps}$, the rest of the quantities are all expressed in units of range. We assume that m satellites are tracked and thus $p, s \in \{h | h = 1, \dots, m\}$, with $p \neq s$.

If we make use of the more compact multi-frequency vector notation $\Delta\phi_u^{ps} = [\Delta\phi_{u,1}^{ps}, \dots, \Delta\phi_{u,f}^{ps}]^T$, $\Delta p_u^{ps} = [\Delta p_{u,1}^{ps}, \dots, \Delta p_{u,f}^{ps}]^T$, $\mu = [\mu_1, \dots, \mu_f]^T$, $z_u^{ps} = [z_{u,1}^{ps}, \dots, z_{u,f}^{ps}]^T$, $\delta^{ps} = [\delta_{,1}^{ps}, \dots, \delta_{,f}^{ps}]^T$, and $d^{ps} = [d_{,1}^{ps}, \dots, d_{,f}^{ps}]^T$, we may write (1) as

$$\begin{aligned}\Delta\phi_u^{ps} &= e \Delta\rho_u^{ps} - \mu \iota_u^{ps} - e dt^{ps} + \Lambda (z_u^{ps} - \delta^{ps}) \\ \Delta p_u^{ps} &= e \Delta\rho_u^{ps} + \mu \iota_u^{ps} - e dt^{ps} - d^{ps}\end{aligned}\quad (2)$$

where $e = [1, \dots, 1]^T$, $\Lambda = \text{diag}(\lambda_1, \dots, \lambda_f)$, and $\Delta\rho_u^{ps} = g^{psT} \Delta x_u$. The user observation equations (2) do not contain enough information to solve for an integer ambiguity resolved user position. This would become possible though, were information about the satellite clocks, dt^{ps} , and satellite biases, δ^{ps} and d^{ps} , be given. Using such externally provided information to correct the observations as

$$\begin{aligned}\Delta\phi_u^{ps} &= \Delta\phi_u^{ps} + e dt^{ps} + \Lambda \delta^{ps} \\ \Delta p_u^{ps} &= \Delta p_u^{ps} + e dt^{ps} + d^{ps}\end{aligned}\quad (3)$$

results in user-equations that take the form

$$\begin{aligned}\Delta\phi_u^{ps} &= e \Delta\rho_u^{ps} - \mu \iota_u^{ps} + \Lambda z_u^{ps} \\ \Delta p_u^{ps} &= e \Delta\rho_u^{ps} + \mu \iota_u^{ps}\end{aligned}\quad (4)$$

This system is now in a form that can be used to solve for the integer ambiguity resolved *user* parameters Δx_u and ι_u . Hence, with externally provided corrections dt^{ps} , δ^{ps} , and d^{ps} , the user system of observation equations (4) can be solved as a mixed-integer system of equations, thereby profiting from the integerness of $z_u^{ps} \in \mathbb{Z}^f$. This is the basic idea of single-receiver, IAR-enabled, positioning.

The operationalization of this basic idea is somewhat more involved however. This is due to the fact that the above needed parameters dt^{ps} , δ^{ps} , d^{ps} *cannot* be determined as such. GNSS-data is namely not capable of providing these 'absolute' parameters, but instead only estimable functions that can *act* as such. These estimable parameters, denoted with a tilde as $\tilde{d}t^{ps}$, $\tilde{\delta}^{ps}$, \tilde{d}^{ps} , achieve the same goal, namely of enabling the construction of a user system of observation equations that is in mixed-integer form. Thus although they are not the original absolute parameters,

$$\tilde{d}t^{ps} \neq dt^{ps}, \tilde{\delta}^{ps} \neq \delta^{ps}, \tilde{d}^{ps} \neq d^{ps}\quad (5)$$

they still do the job in ensuring that the user can work with integer ambiguities. When they are used to correct the user-observations as

$$\begin{aligned}\Delta\tilde{\phi}_u^{ps} &= \Delta\phi_u^{ps} + e \tilde{d}t^{ps} + \Lambda \tilde{\delta}^{ps} \\ \Delta\tilde{p}_u^{ps} &= \Delta p_u^{ps} + e \tilde{d}t^{ps} + \tilde{d}^{ps}\end{aligned}\quad (6)$$

the user equations take the form

$$\begin{aligned}\Delta\tilde{\phi}_u^{ps} &= e \Delta\tilde{\rho}_u^{ps} - \mu \tilde{\iota}_u^{ps} + \Lambda \tilde{z}_u^{ps} \\ \Delta\tilde{p}_u^{ps} &= e \Delta\tilde{\rho}_u^{ps} + \mu \tilde{\iota}_u^{ps}\end{aligned}\quad (7)$$

with integer $\tilde{z}_u^{ps} \in \mathbb{Z}^f$. Thus the structure of these equations is indeed identical to that of the mixed-integer system (4), be it that the interpretation of the estimable parameters in (7) is different from those of (4). This difference in parameter interpretation is important and it is due to the differences in (5).

It is the goal of the present contribution to provide an analytical study of the *estimable* PPP-RTK corrections $\tilde{d}t^{ps}$, $\tilde{\delta}^{ps}$, and \tilde{d}^{ps} , as well as of their impact on the user ambiguity resolution performance. In Sect. 2 we start by introducing single-station PPP-RTK, while in Sect. 3 we warn for the pitfalls that exist when evaluating the PPP-RTK corrections on an individual basis. The results of Sect. 2 are generalized in Sect. 4 and Sect. 5, respectively, to the geometry-free (GF) and geometry-based (GB) network case. This is done in network ambiguity-float as well as in network ambiguity-fixed mode. Next to the insight that is provided by the analytical solutions, the closed form expressions of the variance matrices also demonstrate how the corrections depend on network parameters such as number of epochs, number of stations, number of satellites, and

number of frequencies. As a result we are able to describe in a qualitative sense how the user ambiguity resolution performance is driven by the data from the different network scenarios. A summary with conclusions is finally provided for in Sect. 6.

2 Single-Station PPP-RTK

Although estimators of the PPP-RTK corrections $\tilde{d}t^{ps}$, $\tilde{\delta}^{ps}$, and \tilde{d}^{ps} are usually computed from an external *network*, they can—as the below will show—be obtained from the data of a single station as well.

2.1 Single-station corrections

The observation equations of a single reference station r follow by replacing the user index u in (2) by r ,

$$\begin{aligned}\Delta\phi_r^{ps} &= e(\Delta\rho_r^{ps} - dt^{ps}) - \mu\iota_r^{ps} + \Lambda(z_r^{ps} - \delta^{ps}) \\ \Delta p_r^{ps} &= e(\Delta\rho_r^{ps} - dt^{ps}) + \mu\iota_r^{ps} - d^{ps}\end{aligned}\quad (8)$$

These equations are underdetermined as there are $2f$ equations in $3f+3$ unknowns. The rank defect is $f+3$. There are many different ways to eliminate a rank defect, each with a different interpretation of the resulting estimable parameters. These different sets of estimable parameters are linked by \mathcal{S} -transformations (Baarda, 1973; Teunissen, 1985). Examples of such different sets in the context of PPP-RTK can be found in (Teunissen et al, 2010; Zhang et al, 2011; Lannes and Teunissen, 2011; Odijk et al, 2012) and (Teunissen and Khodabandeh, 2015).

To eliminate the rank defect of the above system (8), we first lump the parameters that have common coefficients,

$$\rho_r^{ps} := \Delta\rho_r^{ps} - dt^{ps}, \quad a_r^{ps} := z_r^{ps} - \delta^{ps}\quad (9)$$

As this takes care of $f+1$ rank defects, there are still 2 defects that need to be taken care of. This will be done by applying the ionosphere-free/geometry-free decomposition of the code bias d^{ps} ,

$$d^{ps} = [e, \mu, E] \begin{bmatrix} d_{IF}^{ps} \\ d_{GF}^{ps} \\ \tilde{d}^{ps} \end{bmatrix}, \quad \text{with } [e, \mu, E]^{-1} = \begin{bmatrix} \mu_{IF}^T \\ \mu_{GF}^T \\ E^- \end{bmatrix}\quad (10)$$

where

$$\begin{aligned}\mu_{IF} &= \frac{1}{\mu_2 - \mu_1} [\mu_2, -\mu_1, 0, \dots, 0]^T \\ \mu_{GF} &= \frac{1}{\mu_2 - \mu_1} [-1, 1, 0, \dots, 0]^T \\ E^- &= E^T (I_f - e\mu_{IF}^T - \mu\mu_{GF}^T)\end{aligned}\quad (11)$$

The $f \times (f-2)$ matrix E is structured by eliminating the first two columns of I_f .

The above decomposition shows that the ionosphere-free and geometry-free combinations d_{IF}^{ps} and d_{GF}^{ps} have the same coefficients as ρ_r^{ps} and ι_r^{ps} , namely e and μ , respectively. Hence, a further lumping can take place, thus taking care of the remaining two rank defects. Substitution of (10) into (8) gives therefore, together with (9), the full-rank single-station model as

$$\begin{aligned}\mathbb{E}(\phi_r^{ps}) &= e\tilde{\rho}_r^{ps} - \mu\tilde{\iota}_r^{ps} + \Lambda\tilde{a}_r^{ps} \\ \mathbb{E}(p_r^{ps}) &= e\tilde{\rho}_r^{ps} + \mu\tilde{\iota}_r^{ps} - E\tilde{d}^{ps}\end{aligned}\quad (12)$$

where

$$\begin{aligned}\tilde{\rho}_r^{ps} &= \rho_r^{ps} - d_{IF}^{ps} \\ \tilde{a}_r^{ps} &= a_r^{ps} + \Lambda^{-1}(e d_{IF}^{ps} - \mu d_{GF}^{ps}) \\ \tilde{\iota}_r^{ps} &= \iota_r^{ps} - d_{GF}^{ps}\end{aligned}\quad (13)$$

The estimable parameters in the above system can be interpreted as a biased range $\tilde{\rho}_r^{ps}$, a biased ambiguity \tilde{a}_r^{ps} , and a biased ionospheric delay $\tilde{\iota}_r^{ps}$. However, note that with the definitions

$$d\tilde{t}^{ps} := -\tilde{\rho}_r^{ps} \quad \text{and} \quad \tilde{\delta}^{ps} := -\tilde{a}_r^{ps}\quad (14)$$

the ‘range’ and ‘ambiguity’ can likewise be interpreted as a biased clock $d\tilde{t}^{ps}$ and a biased phase-bias $\tilde{\delta}^{ps}$, thus giving instead of (13), the estimable parameters

$$\begin{aligned}d\tilde{t}^{ps} &= dt^{ps} + d_{IF}^{ps} - \Delta\rho_r^{ps} \\ \tilde{\delta}^{ps} &= \delta^{ps} - \Lambda^{-1}(e d_{IF}^{ps} - \mu d_{GF}^{ps}) - z_r^{ps} \\ \tilde{\iota}_r^{ps} &= \iota_r^{ps} - d_{GF}^{ps}\end{aligned}\quad (15)$$

The corresponding system of observation equations now reads instead of (12),

$$\begin{aligned}\mathbb{E}(\phi_r^{ps}) &= -e d\tilde{t}^{ps} - \mu\tilde{\iota}_r^{ps} - \Lambda\tilde{\delta}^{ps} \\ \mathbb{E}(p_r^{ps}) &= -e d\tilde{t}^{ps} + \mu\tilde{\iota}_r^{ps} - E\tilde{d}^{ps}\end{aligned}\quad (16)$$

As this is an invertible system of $2f$ equations in $2f$ unknowns per satellite pair ps , its solution follows after inversion as (cf. 10)

$$\begin{aligned}\hat{d\tilde{t}}^{ps} &= -\mu_{IF}^T p_r^{ps} \\ \hat{\tilde{\delta}}^{ps} &= -\Lambda^{-1}[\phi_r^{ps} + (\mu\mu_{GF}^T - e\mu_{IF}^T) p_r^{ps}] \\ \hat{\tilde{d}}^{ps} &= -E^- p_r^{ps} \\ \hat{\tilde{\iota}}_r^{ps} &= +\mu_{GF}^T p_r^{ps}\end{aligned}\quad (17)$$

In the following the *user-aiding* functionality of each of these estimators is described.

2.2 The individual corrections applied

To show the effect that each of the PPP-RTK corrections

$$d\tilde{t}^{ps}, \tilde{\delta}^{ps}, \quad \text{and} \quad \tilde{d}^{ps}\quad (18)$$

has, we apply them sequentially to the user observation equations

$$\begin{aligned}\mathbb{E}(\phi_u^{ps}) &= e\tilde{\rho}_u^{ps} - \mu\tilde{\iota}_u^{ps} + \Lambda\tilde{a}_u^{ps} \\ \mathbb{E}(p_u^{ps}) &= e\tilde{\rho}_u^{ps} + \mu\tilde{\iota}_u^{ps} - E\tilde{d}^{ps}\end{aligned}\quad (19)$$

2.2.1 Clock \tilde{dt}^{ps} provides positional link

For the expectation of the clock correction we have (cf. 15),

$$E(\hat{dt}^{ps}) = \tilde{dt}^{ps} = dt^{ps} + d_{IF}^{ps} - \Delta\rho_r^{ps} \quad (20)$$

Application to (19) gives

$$\begin{aligned} E(\phi_u^{ps} + e \hat{dt}^{ps}) &= e \Delta\rho_{ru}^{ps} - \mu \tilde{t}_u^{ps} + \Lambda \tilde{a}_u^{ps} \\ E(p_u^{ps} + e \hat{dt}^{ps}) &= e \Delta\rho_{ru}^{ps} + \mu \tilde{t}_u^{ps} - E \tilde{d}^{ps} \end{aligned} \quad (21)$$

with $\Delta\rho_{ru}^{ps} = \tilde{\rho}_u^{ps} - \tilde{\rho}_r^{ps} = \Delta\rho_u^{ps} - \Delta\rho_r^{ps}$ being the double-differenced (DD) geometric/tropospheric delay's increment. This shows, when comparing (21) with (19), that the satellite clock correction has the function to establish a positional link between user u and reference r .

2.2.2 Phase-bias $\tilde{\delta}^{ps}$ provides ambiguity link

Although (21) is solvable for the user's position, it is not yet in mixed-integer form, since $\tilde{a}_u^{ps} \notin \mathbb{Z}^f$. To enable user integer ambiguity resolution, the satellite phase-bias $\tilde{\delta}^{ps}$ is needed. For the expectation of the phase-bias correction we have (cf. 15)

$$E(\hat{\delta}^{ps}) = \tilde{\delta}^{ps} = \delta^{ps} + \Lambda^{-1}(\mu d_{GF}^T - e d_{IF}^T) - z_r^{ps} \quad (22)$$

Application to (21) gives

$$\begin{aligned} E(\phi_u^{ps} + e \hat{dt}^{ps} + \Lambda \hat{\delta}^{ps}) &= e \Delta\rho_{ru}^{ps} - \mu \tilde{t}_u^{ps} + \Lambda z_{ru}^{ps} \\ E(p_u^{ps} + e \hat{dt}^{ps}) &= e \Delta\rho_{ru}^{ps} + \mu \tilde{t}_u^{ps} - E \tilde{d}^{ps} \end{aligned} \quad (23)$$

with $z_{ru}^{ps} = \tilde{a}_u^{ps} - \tilde{a}_r^{ps} = z_u^{ps} - z_r^{ps}$ being the integer-valued double-differenced (DD) ambiguities. This shows that the satellite phase-bias correction has the function of replacing the noninteger user ambiguity \tilde{a}_u^{ps} by the integer DD ambiguity between user u and reference r , $z_{ru}^{ps} \in \mathbb{Z}^f$.

2.2.3 Code-bias \tilde{d}^{ps} exploits multi-frequency code data

Although (23) is in mixed-integer form, it does not yet fully exploit all information in case $f > 2$. The reason being that in each of the last $(f - 2)$ code equations of (23), the code-biases \tilde{d}^{ps} are treated as unknown parameters. Hence, to have the multi-frequency user-data properly contribute to the user-solution, the code-bias corrections need to be provided as well. The resulting user-equations then finally read

$$\begin{aligned} E(\phi_u^{ps} - \hat{c}_\phi^{ps}) &= e \Delta\rho_{ru}^{ps} - \mu \tilde{t}_u^{ps} + \Lambda z_{ru}^{ps} \\ E(p_u^{ps} - \hat{c}_p^{ps}) &= e \Delta\rho_{ru}^{ps} + \mu \tilde{t}_u^{ps} \end{aligned} \quad (24)$$

with the combined PPP-RTK phase and code corrections, \hat{c}_ϕ^{ps} and \hat{c}_p^{ps} , given as

$$\begin{aligned} \hat{c}_\phi^{ps} &= -e \hat{dt}^{ps} - \Lambda \hat{\delta}^{ps} \\ \hat{c}_p^{ps} &= -e \hat{dt}^{ps} - E \tilde{d}^{ps} \end{aligned} \quad (25)$$

2.3 Single-Baseline RTK

The above has shown that the PPP-RTK corrected user-model is in fact a *DD-like* model. The clock correction establishes the geometry in DD-form and the phase-bias correction establishes the ambiguity in DD-form. The question that comes to the fore is therefore how this DD-like model of the PPP-RTK user compares to the more traditional single-baseline model. The latter is given as

$$\begin{aligned} \Delta\phi_{ru}^{ps} &= e \Delta\rho_{ru}^{ps} - \mu \iota_{ru}^{ps} + \Lambda z_{ru}^{ps} \\ \Delta p_{ru}^{ps} &= e \Delta\rho_{ru}^{ps} + \mu \iota_{ru}^{ps} \end{aligned} \quad (26)$$

with $\Delta\phi_{ru}^{ps} = \phi_u^{ps} - \phi_r^{ps}$ and $\Delta p_{ru}^{ps} = p_u^{ps} - p_r^{ps}$. It follows from subtracting (8) from its user version, i.e. with r replaced by u .

A comparison of the PPP-RTK user model (24) with the single-baseline RTK model (26) shows that the two models are identical except for their ionospheric delay parametrization, \tilde{t}_u^{ps} vs ι_{ru}^{ps} . For users that are interested in positioning, the performance of the two models (24) and (26) will be the same, both in ambiguity-float as well as in ambiguity-fixed mode. Also their ambiguity-resolution performance will be the same. The ambiguity convergence times of the PPP-RTK user-model (24), i.e. its time-to-first-fix, will therefore be comparable to what one is used to with long baseline ambiguity resolution (Blewitt, 1989; Jonkman et al, 2000; Teunissen et al, 2000; Yu et al, 2011; Li et al, 2014).

The difference in ionospheric delay parametrization between (24) and (26) is essential for those users that are interested in ionospheric delay estimation. With the PPP-RTK user-model (24) a biased ionospheric delay $\tilde{t}_u^{ps} = \iota_u^{ps} - d_{GF}^{ps}$ is obtained, whereas an unbiased DD delay ι_{ru}^{ps} is estimated with the single baseline model (26). In contrast to the single-baseline model, the PPP-RTK user-model would thus be able to provide absolute ionospheric delays if d_{GF}^{ps} would be available, e.g. through calibration (Schaer, 1999).

2.3.1 Ionospheric delay \tilde{t}_r^{ps} to allow for improved IAR

From a positioning perspective, the single-baseline model (26) has the advantage over (24) in that it is parametrized in the *relative* ionospheric delay ι_{ru}^{ps} . Hence, it allows for a further strengthening by making use of the spatial correlation of the ionospheric delays (Odijk, 2002; Grejner-Brzezinska et al, 2007; Wielgosz et al, 2008). This is not possible with the PPP-RTK user-model (24).

To make this possible, an additional ionospheric correction is needed. As

$$E(\hat{\iota}_r^{ps}) = \tilde{t}_r^{ps} = \iota_r^{ps} - d_{GF}^{ps} \quad (27)$$

provision of this ionospheric correction to the user gives

$$\begin{aligned} E(\phi_u^{ps} - \hat{c}_\phi^{ps} + \mu \hat{l}_r^{ps}) &= e \Delta \rho_{ru}^{ps} - \mu l_{ru}^{ps} + \Lambda z_{ru}^{ps} \\ E(p_u^{ps} - \hat{c}_p^{ps} - \mu \hat{l}_r^{ps}) &= e \Delta \rho_{ru}^{ps} + \mu l_{ru}^{ps} \end{aligned} \quad (28)$$

in which the DD ionospheric delay is recognized as $l_{ru}^{ps} = \tilde{l}_u^{ps} - \tilde{l}_r^{ps} = l_u^{ps} - l_r^{ps}$. Compare (28) with (26). Thus with the ionospheric delay provided as an extra user-correction, the PPP-RTK user-model (28) now has the same capabilities as the single baseline model (26). In this contribution though, we restrict attention to the currently more customary case of providing only the PPP-RTK corrections $\hat{d}t^{\hat{ps}}$, $\hat{\delta}^{\hat{ps}}$, and $\hat{d}^{\hat{ps}}$.

3 Pitfalls in analyzing an *individual* correction

3.1 PPP-RTK corrections in combined-form

The above has shown what roles are taken up by the individual PPP-RTK corrections $\hat{d}t^{\hat{ps}}$, $\hat{\delta}^{\hat{ps}}$, and $\hat{d}^{\hat{ps}}$. But what matters, of course, is their combined effect. The comparison between the PPP-RTK model and the single-baseline model has made this clear as well. In the following we will refer to the corrections

$$\begin{aligned} \hat{c}_\phi^{ps} &= -e \hat{d}t^{\hat{ps}} - \Lambda \hat{\delta}^{\hat{ps}} \\ \hat{c}_p^{ps} &= -e \hat{d}t^{\hat{ps}} - E \hat{d}^{\hat{ps}} \end{aligned} \quad (29)$$

as the PPP-RTK corrections in combined form. With the aid of (17) it is not difficult to verify that

$$\begin{aligned} \hat{c}_\phi^{ps} &= \phi_r^{ps} + \mu \hat{l}_r^{ps} \\ \hat{c}_p^{ps} &= p_r^{ps} - \mu \hat{l}_r^{ps} \end{aligned} \quad (30)$$

This shows that the combined PPP-RTK corrections represent a biased version of the original reference station observations. This bias explains the presence of the biased ionospheric delay \tilde{l}_u^{ps} in the PPP-RTK model (24). It can be eliminated if next to $\hat{d}t^{\hat{ps}}$, $\hat{\delta}^{\hat{ps}}$, and $\hat{d}^{\hat{ps}}$, also the ionospheric delay takes part in the corrections. The combined correction then takes the form

$$\begin{aligned} \hat{c}_\phi^{ps} &= \hat{c}_\phi^{ps} - \mu \hat{l}_r^{ps} = \phi_r^{ps} \\ \hat{c}_p^{ps} &= \hat{c}_p^{ps} + \mu \hat{l}_r^{ps} = p_r^{ps} \end{aligned} \quad (31)$$

in which case a complete correspondence with the single-baseline model is obtained. For a quick reference, a brief comparison between the single-station PPP-RTK setup and the single-baseline RTK setup is given in Table 1.

3.2 Individual vs combined corrections

When evaluating the generation of PPP-RTK corrections, it is usually the individual corrections that are

Table 1 User's single-station PPP-RTK setup compared to the standard DD single-baseline setup

	PPP-RTK	Single-baseline
Corrections	$\hat{d}t^{\hat{ps}}, \hat{\delta}^{\hat{ps}}, \hat{d}^{\hat{ps}}$	ϕ_r^{ps}, p_r^{ps}
Comb.-form	$\hat{c}_\phi^{ps} = -e \hat{d}t^{\hat{ps}} - \Lambda \hat{\delta}^{\hat{ps}}$ $\hat{c}_p^{ps} = -e \hat{d}t^{\hat{ps}} - E \hat{d}^{\hat{ps}}$	$-\phi_r^{ps}$ $-p_r^{ps}$
Corrected observations	$\phi_u^{ps} - \hat{c}_\phi^{ps} = \phi_{ru}^{ps} - \mu \hat{l}_r^{ps}$ $p_u^{ps} - \hat{c}_p^{ps} = p_{ru}^{ps} + \mu \hat{l}_r^{ps}$	$\phi_u^{ps} - \phi_r^{ps} = \phi_{ru}^{ps}$ $p_u^{ps} - p_r^{ps} = p_{ru}^{ps}$
Estimable Parameters	Δx_{ru} z_{ru}^{ps} $\hat{l}_u^{ps} = l_u^{ps} - d_{GF}^{ps}$	Δx_{ru} z_{ru}^{ps} $l_{ru}^{ps} = l_u^{ps} - l_r^{ps}$

judged on quality in the literature, instead of their combined form, see e.g. (Li and Zhang, 2012; Zhang et al, 2013; Li et al, 2013). Such an analysis of the individual corrections is useful if one wants to study the characteristics and estimation quality of the individual parameters $\hat{d}t^{\hat{ps}}$, $\hat{\delta}^{\hat{ps}}$, and $\hat{d}^{\hat{ps}}$. However, from a PPP-RTK application point of view, such an individual analysis is far from sufficient. It is far better to aim at a quality analysis of their combined effect. This is the more so as an analysis restricted to the individual corrections disguises important information that may result in serious pitfalls. Here we give two examples that underline the importance of this viewpoint.

Example 1 (Code-dominated corrections) If we apply the variance propagation law to (17), we obtain the variance matrices of the single-station PPP-RTK corrections as

$$\begin{aligned} D(\hat{d}t^{\hat{ps}}) &= 2 (\mu_{IF}^T C_p \mu_{IF}); \rightarrow \text{code-dominated} \\ D(\hat{\delta}^{\hat{ps}}) &= 2 (\Lambda^{-1} C_\phi \Lambda^{-1} + M C_p M^T) \rightarrow \text{code-dominated} \\ D(\hat{d}^{\hat{ps}}) &= 2 (E^{-1} C_p E^{-1}); \rightarrow \text{code-dominated} \\ D(\hat{l}_r^{\hat{ps}}) &= 2 (\mu_{GF}^T C_p \mu_{GF}); \rightarrow \text{code-dominated} \end{aligned} \quad (32)$$

in which $2C_p$ and $2C_\phi$ are the cofactor matrices for the satellite-differenced pseudorange and carrier-phase, respectively. This result clearly shows that the precision of the individual corrections is governed by the rather poor precision of the code observations. This seems to be at odds however with the quality that the PPP-RTK user-phase corrections are required to have to enable user-ambiguity resolution.

The reason for this apparent inconsistency lies in the *high correlation* that exists between the individual corrections. This becomes clear if we express the phase-bias solution as

$$\hat{\delta}^{\hat{ps}} = -\Lambda^{-1} (\phi_r^{ps} + e \hat{d}t^{\hat{ps}} + \mu \hat{l}_r^{ps}) \quad (33)$$

This expression shows that the phase-bias solution is indeed highly correlated with the clock- and ionospheric

corrections. It is this high correlation that ‘repairs’ the situation when forming the combined PPP-RTK user-phase correction. Instead of the code-dominated individual corrections, the precise combined correction

$$\hat{c}_\phi^{ps} = -\Lambda \hat{\delta}^{\tilde{ps}} - e \hat{dt}^{\tilde{ps}} - \mu \hat{l}_r^{\tilde{ps}} \quad (34)$$

is obtained, the precision of which will be at the phase-noise level instead of at the code-noise level.

The conclusion reads therefore that the *combined form* of the PPP-RTK corrections should be used for performance evaluation and not the code-noise dominated time series of the individual PPP-RTK corrections. Note that the same conclusion is reached if one would follow the derivation in ionosphere-free form. Hence, the conclusion is not dependent on whether or not the ionospheric correction is provided.

Example 2 (Perfectly known phase-biases) As PPP-RTK users may not always use corrections from one single provider, we now consider a case that can be considered as an example where corrections of two different providers are used. From the first provider, the single-station, the user uses the earlier derived single-station clock- and ionospheric solutions, $\hat{dt}^{\tilde{ps}}$ and $\hat{l}_r^{\tilde{ps}}$. And from a second provider the user obtains very precise phase-bias corrections, denoted as $\tilde{\delta}^{ps*}$. For argument-sake the phase biases $\tilde{\delta}^{ps*}$ are assumed so precise that they can be considered non-random for this example.

The corresponding combined corrections now read

$$\begin{aligned} \hat{c}_\phi^{ps*} &= -e \hat{dt}^{\tilde{ps}} - \mu \hat{l}_r^{\tilde{ps}} - \Lambda \tilde{\delta}^{ps*} \\ \hat{c}_p^{ps} &= -e \hat{dt}^{\tilde{ps}} + \mu \hat{l}_r^{\tilde{ps}} \end{aligned} \quad (35)$$

Note that while the code-correction \hat{c}_p^{ps} remains unchanged, the phase-correction \hat{c}_ϕ^{ps*} differs from its single-station counterpart \hat{c}_ϕ^{ps} as,

$$\hat{c}_\phi^{ps*} = \hat{c}_\phi^{ps} + \Lambda \varepsilon^{ps} = \phi_r^{ps} + \Lambda \varepsilon^{ps} \quad (36)$$

in which $\varepsilon^{ps} = \hat{\delta}^{\tilde{ps}} - \tilde{\delta}^{ps*}$ is zero mean with dispersion $D(\hat{\delta}^{\tilde{ps}})$. Application of the variance propagation law gives

$$D(\hat{c}_\phi^{ps*}) = \Lambda D(\hat{\delta}^{\tilde{ps}}) \Lambda - D(\phi_r^{ps}) \rightarrow \text{code-dominated} \quad (37)$$

This shows that the provision of the perfectly known phase-bias $\tilde{\delta}^{ps*}$ has turned the previously very precise phase-correction \hat{c}_ϕ^{ps} into a *less precise* code-dominated phase-correction \hat{c}_ϕ^{ps*} .

So what have we gained? Again one should not fall in the trap of making the judgment on the basis of an individual correction. That is, one should consider the PPP-RTK corrections in their combined form. By

doing so, one will note the role played by the non-zero correlation between ε^{ps} and the code-corrections \hat{c}_p^{ps} .

Indeed, if \hat{z}_{ru}^{ps} and \hat{z}_{ru}^{ps*} denote the two types of float solutions of the user-ambiguities based on the two sets of corrections $\hat{c}_\phi^{ps}, \hat{c}_p^{ps}$ and $\hat{c}_\phi^{ps*}, \hat{c}_p^{ps}$, respectively, then it follows from (36) that ε^{ps} gets fully absorbed in the estimator of the user DD ambiguity z_{ru}^{ps} . Hence, the float solution of all user parameters except the ambiguities remains unchanged, while the user ambiguity solution simply changes as $\hat{z}_{ru}^{ps*} = \hat{z}_{ru}^{ps} - \varepsilon^{ps}$. Since the covariance of \hat{z}_{ru}^{ps} and ε^{ps} is given by $D(\hat{\delta}^{\tilde{ps}})$, application of the variance propagation law gives

$$D(\hat{z}_{ru}^{ps*}) = D(\hat{z}_{ru}^{ps}) - D(\hat{\delta}^{\tilde{ps}}) \quad (38)$$

thus showing that a more precise ambiguity solution is obtained. This shows that despite the poorer precision of the phase-correction (\hat{c}_ϕ^{ps*} vs \hat{c}_ϕ^{ps}), the use of $\tilde{\delta}^{ps*}$ does result in more precise user ambiguities and therefore in an improved ambiguity resolution performance. This again demonstrates that one should use the combined form of the PPP-RTK corrections, i.e. $\hat{c}_\phi^{ps*}, \hat{c}_p^{ps}$, for performance evaluation and not the individual corrections.

4 Geometry-Free Network Derived Corrections

4.1 Multivariate formulation

So far we restricted ourselves to the observation equations of a single network station r . We now extend the results to n network stations. We use a multivariate formulation and therefore define the undifferenced phase observation vector of station r as $\phi_r = [\phi_{r,1}^T, \dots, \phi_{r,f}^T] \in \mathbb{R}^{fm}$, $\phi_{r,j} = [\Delta\phi_{r,j}^1, \dots, \Delta\phi_{r,j}^m]$, $j = 1, \dots, f$, with a likewise definition for the code observation vector p_r . For the n stations, the network observation matrices are defined as $\Phi = [\phi_1, \dots, \phi_n]$ and $P = [p_1, \dots, p_n]$. The compact multivariate formulation of the full-rank, multi-epoch, network observation equations becomes then

$$\begin{aligned} E((I_f \otimes D_m^T) \Phi(i)) &= \\ (e \otimes I_{m-1}) \tilde{\rho}(i) - (\mu \otimes I_{m-1}) \tilde{i}(i) + (\Lambda \otimes I_{m-1}) \tilde{A} \\ E((I_f \otimes D_m^T) P(i)) &= \\ (e \otimes I_{m-1}) \tilde{\rho}(i) + (\mu \otimes I_{m-1}) \tilde{i}(i) - (E \otimes I_{m-1}) \tilde{d} e_n^T \end{aligned} \quad (39)$$

where D_m^T denotes an $(m-1) \times m$ between-satellite differencing matrix. The index i refers to the epoch at which the observations are collected. This system generalizes the single-station system (12). The compact and insightful formulation of (39) is in a large part due to the application of the efficient Kronecker product \otimes (Henderson et al, 1983), which was first introduced for GNSS models in (Teunissen, 1997a).

Table 2 Network's parameters in index-, vector- and multivariate-forms ($p \neq s$)

	Index-form	Vector-form	Multivariate-form
Non-dispersive SD delays	$\tilde{\rho}_r^{ps} = \rho_r^{ps} - d_{IF}^{ps}$,	$\tilde{\rho}_r = [\tilde{\rho}_r^{p1}, \dots, \tilde{\rho}_r^{pm}]^T$,	$\tilde{\rho} = [\tilde{\rho}_1, \dots, \tilde{\rho}_n]$
Dispersive SD delays	$\tilde{\iota}_r^{ps} = \iota_r^{ps} - d_{GF}^{ps}$,	$\tilde{\iota}_r = [\tilde{\iota}_r^{p1}, \dots, \tilde{\iota}_r^{pm}]^T$,	$\tilde{\iota} = [\tilde{\iota}_1, \dots, \tilde{\iota}_n]$
Estimable SD ambiguities	$\tilde{a}_r^{ps} = a_r^{ps} - Md^{ps}$,	$\tilde{a}_r = [[\tilde{a}_{r,1}^{p1}, \dots, \tilde{a}_{r,1}^{pm}]^T, \dots, [\tilde{a}_{r,f}^{p1}, \dots, \tilde{a}_{r,f}^{pm}]^T]^T$,	$\tilde{\mathcal{A}} = [\tilde{a}_1, \dots, \tilde{a}_n]$

$$M = \Lambda^{-1}(\mu \mu_{GF}^T - e \mu_{IF}^T)$$

Following (ibid), the above model is referred to as *geometry-free* (GF) since no information about the relative receiver-satellite geometry is present in its design matrix. The matrices $\tilde{\rho}(i)$, $\tilde{\iota}(i)$ and $\tilde{\mathcal{A}}$ contain the network's SD estimable non-dispersive delays, ionospheric delays and ambiguities, respectively (Table 2). The SD estimable code biases on the third frequency and beyond are collected in vector \tilde{d} .

As we assume the station integer ambiguities z_l^{ps} ($l = 1, \dots, n$), the satellite phase biases δ_r^{ps} and the satellite code biases d_r^{ps} of the between-satellite single differences to be time-constant, the time-constant estimable parameters of the above full-rank model are the $f(m-1) \times n$ ambiguity matrix $\tilde{\mathcal{A}}$ and the $(f-2)(m-1) \times 1$ code bias vector \tilde{d} . As before we take station r as the station to define our estimable satellite clock and estimable satellite phase bias, i.e. $\tilde{d}r^{ps}(i) := -\tilde{\rho}_r^{ps}(i)$ and $\tilde{\delta}_r^{ps} := -\tilde{a}_r^{ps}$ (cf. 16). The goal is now to derive the estimators for the network-based PPP-RTK corrections and to analyse the improvements that can so be achieved.

The stochastic model of the network's observables is assumed given as

$$D \begin{bmatrix} (I_f \otimes D_m^T) \phi_r(i) \\ (I_f \otimes D_m^T) p_r(i) \end{bmatrix} = c_r^2 \begin{bmatrix} C_\phi & 0 \\ 0 & C_p \end{bmatrix} \otimes C_s(i) \quad (40)$$

in which $C_s(i) = D_m^T C_S(i) D_m$, with $C_S(i)$ the $m \times m$ co-factor matrix that captures the satellite elevation dependency at epoch i . The scalar c_r^2 ($r = 1, \dots, n$) is a receiver-dependent co-factor. In this study all receivers are assumed to be of the same quality and thus $c_r^2 = 1$ for all r . The $f \times f$ positive-definite matrices C_ϕ and C_p are the co-factor matrices of the phase and code observable types, respectively.

4.2 Geometry-free network redundancy

To identify the relevance of the *network* for PPP-RTK, we need to understand how its redundancy contributes to the best linear unbiased estimator (BLUE) of the PPP-RTK corrections. The network redundancy is defined here as the number of its observations minus the

number of its estimable parameters. Would one discard this redundancy, then the network-derived corrections simply follow from the single-station solutions (31). In multivariate form they then read

$$\begin{bmatrix} \tilde{\hat{c}}_\phi(i) \\ \tilde{\hat{c}}_p(i) \end{bmatrix} = \begin{bmatrix} (I_f \otimes D_m^T) \phi_r(i) \\ (I_f \otimes D_m^T) p_r(i) \end{bmatrix} \quad (41)$$

They can be further improved however by exploiting the network redundancy. For the network redundancy, we discriminate between two cases:

- *Ambiguity float*: the case that the DD ambiguities are treated as real-valued parameters; and
- *Ambiguity fixed*: the case that the DD ambiguities are successfully resolved as integers.

For the geometry-free (GF) network model (39), the ambiguity-float k -epoch redundancy is given as

$$\begin{aligned} \# \text{ GF-float redundancy} = \\ \{k(f-2)(n-1) + (k-1)(fn+f-2)\}(m-1) \end{aligned} \quad (42)$$

We now show how this redundancy is built up from the various elements of the network. For a quick reference,

Table 3 Geometry-free network redundancy brought by the ambiguity-float and -fixed scenarios, giving the total size of $2(kn-1)(f-1)(m-1)$

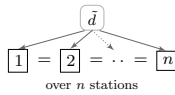
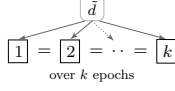
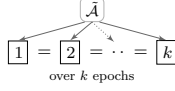
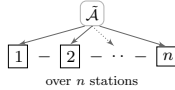
Scenario	Type	Size
(1) single-epoch ($f > 2, n > 1$)		$(f-2)(n-1)(m-1)$
(2) multi-epoch ($f > 2, k > 1$)		$(k-1)(f-2)(m-1)n$
(3) multi-epoch ($k > 1$)		$(k-1)f(m-1)n$
# Ambiguity-float		$\{k(f-2)(n-1) + (k-1)(fn+f-2)\}(m-1)$
(4) network-IAR		$f(n-1)(m-1)$
# Ambiguity-fixed		$2(kn-1)(f-1)(m-1)$

Table 4 (Co)Variance matrices of the ambiguity-float geometry-free (GF) corrections. The ambiguities, phase and code biases are assumed constant over k epochs.

$Q_{d\hat{t}\hat{t}(i)}^{GF}$	$= [\frac{1}{k}c_{\hat{\rho}_2}^2 \otimes \bar{C}_s] + [c_{\hat{\rho}}^2 \otimes (C_s(i) - \frac{1}{k}\bar{C}_s)] - [\frac{n-1}{kn}\Delta c_{\hat{\rho}}^2 \otimes \bar{C}_s]$
$Q_{\hat{\delta}\hat{\delta}}^{GF}$	$= [\frac{1}{k}A^{-1}(C_\phi + [e, -\mu]Q_{[\hat{\rho}_2, i_2]}[e, -\mu]^T)A^{-1} \otimes \bar{C}_s] - [\frac{n-1}{kn}A^{-1}([e, -\mu]\Delta Q_{[\hat{\rho}, i]}[e, -\mu]^T)A^{-1} \otimes \bar{C}_s]$
$Q_{\hat{d}\hat{d}}^{GF}$	$= \frac{1}{kn}(E^-C_pE^{-T}) \otimes \bar{C}_s$
$Q_{d\hat{\delta}\hat{\delta}(i)}^{GF}$	$= -[\frac{1}{k}(c_{\hat{\rho}_2}^2 e^T - c_{\hat{\rho}i_2} \mu^T)A^{-1} \otimes \bar{C}_s] + [\frac{n-1}{kn}(\Delta c_{\hat{\rho}}^2 e^T - \Delta c_{\hat{\rho}i} \mu^T)A^{-1} \otimes \bar{C}_s]$
$Q_{d\hat{t}\hat{t}(i)}^{GF}$	$= \frac{1}{kn}(\mu_{IF}^T C_p E^{-T}) \otimes \bar{C}_s$
$Q_{\hat{\delta}\hat{d}}^{GF}$	$= \frac{1}{kn}A^{-1}(MC_pE^{-T}) \otimes \bar{C}_s$

$Q_{[\hat{\rho}, i]} = \begin{bmatrix} c_{\hat{\rho}}^2 & c_{\hat{\rho}i} \\ c_{\hat{\rho}i} & c_i^2 \end{bmatrix}$	$= ([e, \mu]^T C_p^{-1} [e, \mu])^{-1};$	$Q_{[\hat{\rho}_2, i_2]} = \begin{bmatrix} c_{\hat{\rho}_2}^2 & c_{\hat{\rho}i_2} \\ c_{\hat{\rho}i_2} & c_{i_2}^2 \end{bmatrix}$	$= [\mu_{IF}, \mu_{GF}]^T C_p [\mu_{IF}, \mu_{GF}];$	$\Delta Q_{[\hat{\rho}, i]} = Q_{[\hat{\rho}_2, i_2]} - Q_{[\hat{\rho}, i]} = \begin{bmatrix} \Delta c_{\hat{\rho}}^2 & \Delta c_{\hat{\rho}i} \\ \Delta c_{\hat{\rho}i} & \Delta c_i^2 \end{bmatrix}$
$Q_{[\hat{\rho}, i]} = \begin{bmatrix} c_{\hat{\rho}}^2 & c_{\hat{\rho}i} \\ c_{\hat{\rho}i} & c_i^2 \end{bmatrix}$	$= ([\tilde{e}, \tilde{\mu}]^T \text{blkdiag}(C_\phi^{-1}, C_p^{-1}) [\tilde{e}, \tilde{\mu}])^{-1}$			

a summary of the elements building up the network redundancy is provided in Table 3.

In the single-epoch, multi-frequency case, the network redundancy stems from the fact that all single-station solutions of the estimable code biases \tilde{d}^{ps} have the *same* mean, that is

$$E(E^-p_l^{ps}) = -\tilde{d}^{ps}, \quad l = 1, \dots, n \quad (43)$$

or

$$E(E^-p_{ri}^{ps}) = 0, \quad l \neq r \quad (44)$$

In multivariate form this reads as

$$E((E^- \otimes D_m^T) P D_n) = 0 \quad (45)$$

in which D_n is the $n \times (n-1)$ between-station differencing matrix. Thus in the single-epoch case the redundancy is $(f-2)(m-1)(n-1)$. Hence, there is no redundancy in the single-station case ($n=1$, see previous section) and no redundancy in case of dual-frequency data ($f=2$).

In case of k epochs, all the additional single-station solutions of \tilde{d}^{ps} (of the second epoch and beyond) have the *same* mean as those of (43). This is the case since the estimable code biases are assumed to be constant in time. This gives an additional redundancy of $(k-1)$ times $(f-2)(m-1)n$. Similarly, an additional redundancy of $(k-1)$ times $f(m-1)n$ is then also obtained due to the time-constancy of the ambiguity matrix $\tilde{\mathcal{A}} = [\tilde{a}_1, \dots, \tilde{a}_n]$. Summing these redundancies up gives (42).

Now we consider the ambiguity-fixed network redundancy. It is given as

$$\# \text{ GF-fixed redundancy} = 2(kn-1)(f-1)(m-1) \quad (46)$$

Compare this to the ambiguity-float redundancy (42) and note that it is $f(m-1)(n-1)$ larger. This increase in redundancy is due to the successfully resolved integer ambiguities. As the between-station differences of the

single-station solutions of the estimable SD ambiguities $\tilde{a}_{ri}^{ps} = \tilde{a}_i^{ps} - \tilde{a}_r^{ps}$ have *integer-valued* means, we have

$$E(\Lambda^{-1} \phi_{rl}^{ps} + M p_{rl}^{ps}) = z_{rl}^{ps} \in \mathbb{Z}, \quad l \neq r \quad (47)$$

or in multivariate form

$$E((\Lambda^{-1} \otimes D_m^T) \Phi D_n + (M \otimes D_m^T) P D_n) \in \mathbb{Z}^{f(m-1)(n-1)} \quad (48)$$

with $M = \Lambda^{-1}(\mu \mu_{GF}^T - e \mu_{IF}^T)$. Hence, successfully resolving the integer ambiguities results in an additional $f(m-1)(n-1)$ condition equations and ditto redundancy. The total ambiguity-fixed redundancy is therefore given by (46). Note that now there already exists redundancy when $k=1$, $f=2$ and $n>1$, this in contrast to the ambiguity-float case (cf. 42). However, for $k=1$, $f=2$, and $n=1$ there is still no redundancy as the single-station case does not enable the formation of integer ambiguities. For $n>1$ such integers can be formed and the redundancy becomes then, for example, for $k=1$, $f=2$ and $n=2$ equal to $2(m-1)$, which is indeed the number of dual-frequency DD ambiguities that can be formed in case of a single baseline.

4.3 The Ambiguity-Float GF corrections

In this section we present our analytical analysis of the geometry-free, ambiguity-float network-based PPP-RTK corrections. First we derived the BLUE estimators of the individual PPP-RTK corrections $d\hat{t}^{ps}$, $\hat{\delta}^{ps}$ and \hat{d}^{ps} . Their precision is described by the variance-covariance matrices as given in Table 4. Note that their covariance matrices are given in the table as well. In the table, additional terms, indicated by the Δ -symbol, show up themselves to characterize the contribution of the multi-frequency code data. Thus when $f=2$, they vanish, that is, $\Delta Q_{[\hat{\rho}, i]} = 0$. To gain a better insight into the results, let us start with the dual-frequency case, where the (co)variance matrices corresponding to

the code biases \tilde{d}^{ps} are absent, as in that case E does not exist by definition. In that case, all the (co)variance matrices, except those of the satellite clocks, follow the 1-over- k rule. For not too large k , almost the same rule applies to the variance matrices of the satellite clocks as well, since $(c_{\tilde{\rho}}/c_{\tilde{\rho}_2}) \approx 0$. Let us now consider the multi-frequency case ($f > 2$). As extra frequencies enter, the precision of the satellite clocks and phase biases improves as their (co)variance matrices decrease by a factor governed by $\Delta Q_{[\tilde{\rho}, \tilde{i}]} \neq 0$. Next to those of the satellite clocks and phase biases however, the (co)variance matrices of the code biases \tilde{d}^{ps} enter. They follow the 1-over- kn rule. Thus they are largely driven by both the number of epochs k and stations n .

Based on the individual corrections one can construct the BLUE of the combined corrections, $(\hat{c}_\phi^T, \hat{c}_p^T)^T$ (cf. 29) or $(\hat{c}_\phi^T, \hat{c}_p^T)^T$ (cf. 31). As these two correction types are related as

$$\begin{bmatrix} \hat{c}_\phi \\ \hat{c}_p \end{bmatrix} = \begin{bmatrix} \hat{c}_\phi \\ \hat{c}_p \end{bmatrix} - \begin{bmatrix} -\mu \\ +\mu \end{bmatrix} \iota \quad (49)$$

both can be used for our analytical analysis of the user PPP-RTK positioning performance. The difference of the two type of corrections lies namely in the range of $(-\mu^T, +\mu^T)^T$ and will therefore be completely absorbed by the ionospheric delays of the user. Hence, their difference will not affect the estimation of user-positioning nor that of user-ambiguity resolution. This can alternatively be understood by noting that both type of corrections have the same ionosphere-free combination. Hence, both corrections lead to an identical ionosphere-free user-correction.

In the following we work with the combined corrections $(\hat{c}_\phi^T, \hat{c}_p^T)^T$. First we present their BLUE and then their variance-covariance matrix. The following two averaging operators will be frequently used in the remainder of this contribution

$$\begin{aligned} \text{station-averaging: } (\cdot)_{\bar{r}} &= \frac{1}{n} \sum_{r=1}^n (\cdot)_r, \\ \text{epoch-averaging: } & \quad \quad \quad (50) \end{aligned}$$

$$(\cdot)(\bar{i}) = [I_f \otimes [\sum_{i=1}^k C_S^{-1}(i)]^{-1}] \sum_{i=1}^k [I_f \otimes C_S^{-1}(i)] (\cdot)(i)$$

We also make use of the notations $(\cdot)_{\bar{r}r} = (\cdot)_r - (\cdot)_{\bar{r}}$ and $(\cdot)(\bar{i}\bar{i}) = (\cdot)(i) - (\cdot)(\bar{i})$. Thus in the single-station case we have $(\cdot)_{\bar{r}} = (\cdot)_r$, therefore $(\cdot)_{\bar{r}r} = 0$. Likewise, in the single-epoch case we have $(\cdot)(\bar{i}) = (\cdot)(i)$, therefore $(\cdot)(\bar{i}\bar{i}) = 0$.

Theorem 1 (GF ambiguity-float corrections) *The k -epoch geometry-free ambiguity-float BLUE of the network-derived corrections, at epoch i , is given as*

$$\begin{bmatrix} \hat{c}_{\phi, GF}(i) \\ \hat{c}_{p, GF}(i) \end{bmatrix} = \mathbf{I} - \hat{\mathbf{II}} - \hat{\mathbf{III}} \quad (51)$$

with

$$\begin{aligned} \mathbf{I} &= (I_{2f} \otimes D_m^T) \begin{bmatrix} \phi_r(i) \\ p_r(i) \end{bmatrix} \\ \hat{\mathbf{II}} &= (\mathcal{P}_{[\tilde{e}, \tilde{\mu}]}^\perp \otimes D_m^T) \begin{bmatrix} \phi_r(\bar{i}\bar{i}) \\ p_r(\bar{i}\bar{i}) \end{bmatrix} \\ \hat{\mathbf{III}} &= \begin{bmatrix} 0 \\ (\mathcal{P}_{[e, \mu]}^\perp \otimes D_m^T) p_{\bar{r}r}(\bar{i}) \end{bmatrix} \end{aligned} \quad (52)$$

and the projectors

$$\begin{aligned} \mathcal{P}_{[e, \mu]} &= C_{\tilde{\rho}} C_p^{-1}, \quad \mathcal{P}_{[e, \mu]}^\perp = I_f - \mathcal{P}_{[e, \mu]} \\ \mathcal{P}_{[\tilde{e}, \tilde{\mu}]} &= C_{[\tilde{\phi}, \tilde{p}]} \text{blkdiag}(C_\phi^{-1}, C_p^{-1}) \\ \mathcal{P}_{[\tilde{e}, \tilde{\mu}]}^\perp &= I_{2f} - \mathcal{P}_{[\tilde{e}, \tilde{\mu}]} \end{aligned} \quad (53)$$

where $\tilde{e} = [e^T, e^T]^T$, $\tilde{\mu} = [-\mu^T, \mu^T]^T$, and

$$\begin{aligned} C_{\tilde{\rho}} &= [e, \mu] Q_{[\tilde{\rho}, \tilde{i}]} [e, \mu]^T, \\ Q_{[\tilde{\rho}, \tilde{i}]} &= ([e, \mu]^T C_p^{-1} [e, \mu])^{-1}, \\ C_{[\tilde{\phi}, \tilde{p}]} &= [\tilde{e}, \tilde{\mu}] Q_{[\tilde{\rho}, \tilde{i}]} [\tilde{e}, \tilde{\mu}]^T \\ Q_{[\tilde{\rho}, \tilde{i}]} &= ([\tilde{e}, \tilde{\mu}]^T \text{blkdiag}(C_\phi^{-1}, C_p^{-1}) [\tilde{e}, \tilde{\mu}])^{-1}, \end{aligned} \quad (54)$$

Proof See Appendix. \square

So as to facilitate its interpretation, the GF-correction (51) has been written in terms of three expressions. The first expression \mathbf{I} equals the single-station, single-epoch solution of the previous section (cf. 41), while the second expression $\hat{\mathbf{II}}$ describes the multi-epoch contribution and the third expression $\hat{\mathbf{III}}$ the multi-station contribution. Thus $\hat{\mathbf{II}} = 0$ if $\bar{i} = i$ and $\hat{\mathbf{III}} = 0$ if $\bar{r} = r$.

As the two terms, $\hat{\mathbf{II}}$ and $\hat{\mathbf{III}}$, further adjust the single-station solution, they have a zero mean, $\mathbf{E}(\hat{\mathbf{II}}) = \mathbf{E}(\hat{\mathbf{III}}) = 0$. Thus, although the three-term expression (51) provides the BLUE, any of the following combinations provides a LUE and therefore an unbiased estimator of the corrections: \mathbf{I} , $\mathbf{I} - \hat{\mathbf{II}}$, and $\mathbf{I} - \hat{\mathbf{III}}$.

Note that the third term not only vanishes for $\bar{r} = r$, but also if $f = 2$, since then $\mathcal{P}_{[e, \mu]} = I_2$ and thus $\mathcal{P}_{[e, \mu]}^\perp = 0$. Hence, in the dual-frequency case, not the number of stations, but only the number of epochs contribute to further improving these geometry-free float corrections.

Also note that the third term only contains code data, this in contrast to the first two terms. Hence, if there are more than one station, then only the code data contribute to a further improvement of these GF float corrections.

An important outcome of Theorem 1 is that the combined network correction can indeed be viewed as an *adjusted* version of the observations of a *single* station. Therefore once the corrections are applied to the PPP-RTK user data, the user corrected observation equations can be interpreted *as if* a single baseline is

formed between the user and a network-adjusted reference station.

The precision of the above corrections is obtained after applying the variance propagation law. The result is given in the following lemma.

Lemma 1 (Precision GF ambiguity-float corrections) *The variance matrix of the corrections (51) is given as*

$$D\left(\begin{bmatrix} \hat{\tilde{c}}_{\phi,GF}(i) \\ \hat{\tilde{c}}_{p,GF}(i) \end{bmatrix}\right) = D(\mathbf{I}) - D(\hat{\mathbf{I}}) - D(\hat{\mathbf{I}}\mathbf{I}) \quad (55)$$

with

$$\begin{aligned} D(\mathbf{I}) &= \begin{bmatrix} C_\phi & 0 \\ 0 & C_p \end{bmatrix} \otimes C_s(i) \\ D(\hat{\mathbf{I}}) &= P_{[\hat{e}, \hat{\mu}]}^\perp \begin{bmatrix} C_\phi & 0 \\ 0 & C_p \end{bmatrix} \otimes [C_s(i) - \frac{1}{k} \bar{C}_s] \\ D(\hat{\mathbf{I}}\mathbf{I}) &= \frac{n-1}{n} \begin{bmatrix} 0 & 0 \\ 0 & P_{[\hat{e}, \hat{\mu}]}^\perp C_p \end{bmatrix} \otimes \frac{1}{k} \bar{C}_s \end{aligned} \quad (56)$$

where $\bar{C}_s^{-1} = \frac{1}{k} \sum_{i=1}^k C_s^{-1}(i)$.

Proof Follows by an application of the variance propagation law to (51). \square

This result shows how the precision of the corrections is driven by the various contributing factors, like precision of observables, number of epochs, number of network stations and the frequencies. In the following we will show the extent to which these contributing factors contribute to the precision of the corrections. We will then also show the impact that these corrections are expected to have on the user's ability to perform successful integer ambiguity resolution.

Role of k , n and f : As the code observables are the less precise observables, it is particularly of interest to understand how the precision of the code correction, $D(\hat{\tilde{c}}_{p,GF}(i))$, benefits from increasing number of epochs k , stations n and/or frequencies f . Note that both $D(\hat{\mathbf{I}})$ and $D(\hat{\mathbf{I}}\mathbf{I})$ depend on k , while only $D(\hat{\mathbf{I}}\mathbf{I})$ depends on n . For $k = 1$ the second term vanishes, while for $n = 1$ the third term vanishes. Furthermore, this last term also vanishes if $f = 2$.

A plot of the square root of the mean variance of an individual satellite at zenith (when $c_s(i) = 1$), i.e. $\text{trace}(D(\hat{\tilde{c}}_{p,GF}^s(i)))/f$, is given in Figure 1. It shows that the impact of the number of stations gets less the larger the number of epochs. This can be understood from the contribution of the third term $D(\hat{\mathbf{I}}\mathbf{I})$. Thus only when not too many epochs are used, will the number of stations have a significant effect. For the case of a single station, the third term vanishes, and the variance of the code corrections behaves as $1/k$.

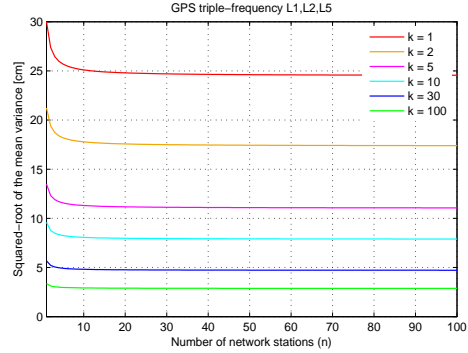


Fig. 1 GPS L1, L2, L5 scenario: the squared-root of the zenith-referenced mean variance of the GF ambiguity-float code corrections as a function of the number of stations n for different number of epochs k ($\sigma_\phi = 3$ [mm], $\sigma_p = 30$ [cm], $c_s = 1$).

4.4 The Ambiguity-Fixed GF Corrections

We now present our results for the geometry-free ambiguity-fixed network-based PPP-RTK corrections. Again we first derived the BLUE estimators of the individual corrections $\tilde{d}t^{ps}$, $\tilde{\delta}^{ps}$ and \tilde{d}^{ps} . Their precision is described by the variance-covariance matrices as given in Table 5. To discuss the table, let us start with the dual-frequency case, where the (co)variance matrices corresponding to the code biases \tilde{d}^{ps} are absent and $\Delta Q_{[\hat{\rho}, \hat{i}]} = 0$. In that case, the (co)variance matrices, corresponding to the satellite phase biases $\tilde{\delta}^{ps}$, are reduced in accordance with the 1-over- n rule. For not too large n however, almost the same rule applies to the variance matrices of the satellite clocks as well, since $(c_{\hat{\rho}}/c_{\hat{\rho}_2}) \approx 0$. Let us now consider the multi-frequency case ($f > 2$). It is remarkable to see that the (co)variance matrices, corresponding to the satellite code biases \tilde{d}^{ps} , remain *unchanged* after network ambiguity resolution. This is indeed due to the fact that the satellite code biases \tilde{d}^{ps} are *uncorrelated* with the float DD ambiguities (Teunissen and Khodabandeh, 2014). Also note, since $\Delta Q_{[\hat{\rho}, \hat{i}]} \neq 0$ when $f > 2$, that the (co)variance matrices of the satellite clocks and phase biases do not follow the 1-over- n improvement anymore.

Based on the individual corrections one can construct the ambiguity-fixed combined corrections $(\tilde{c}_\phi^T, \tilde{c}_p^T)^T$. First we present their estimators and then their variance-covariance matrices.

Theorem 2 (GF ambiguity-fixed corrections) *The k -epoch geometry-free ambiguity-fixed BLUE of the network-derived corrections, at epoch i , is given as*

$$\begin{bmatrix} \tilde{c}_{\phi,GF}(i) \\ \tilde{c}_{p,GF}(i) \end{bmatrix} = \mathbf{I} - \check{\mathbf{I}} \quad (57)$$

with

$$\begin{aligned} \mathbf{I} &= (I_{2f} \otimes D_m^T) \begin{bmatrix} \phi_r(i) \\ p_r(i) \end{bmatrix} \\ \check{\mathbf{I}} &= (P_{[\bar{e}, \bar{\mu}]}^\perp \otimes D_m^T) \begin{bmatrix} \phi_r(\bar{i}) + \tilde{\phi}_{\bar{r}r}(\bar{i}) \\ p_r(\bar{i}) + p_{\bar{r}r}(\bar{i}) \end{bmatrix} \end{aligned} \quad (58)$$

in which the ambiguity-fixed phase data are defined as

$$\begin{aligned} \tilde{\phi}_r &= \phi_r \\ \tilde{\phi}_l &= \phi_l - [A \otimes L] \check{z}_{rl}, \quad l \neq r \end{aligned} \quad (59)$$

with L being an $m \times (m-1)$ matrix formed by removing the p^{th} column of I_m (given p as the pivot satellite).

Proof See Appendix. \square

Compare the above results with that of (51). In particular note that now in the ambiguity-fixed case the time-averaging and the station-averaging have the same contribution to the corrections. In the ambiguity-float case, the contribution from the station-averaging was confined to the code data only (cf. $\hat{\mathbf{I}}$ in 51). In the ambiguity-fixed case however, also the ambiguity-fixed carrier phase data $\tilde{\phi}_l$ acts as pseudorange data and will therefore contribute in a likewise manner in the station-averaging.

The precision of the above corrections is obtained after applying the variance propagation law. The result is given in the following lemma.

Lemma 2 (Precision GF ambiguity-fixed corrections) *The precision of the corrections (57) is given as*

$$\mathbf{D} \left(\begin{bmatrix} \check{\tilde{c}}_{\phi, GF}(i) \\ \check{\tilde{c}}_{p, GF}(i) \end{bmatrix} \right) = \mathbf{D}(\mathbf{I}) - \mathbf{D}(\check{\mathbf{I}}) \quad (60)$$

with

$$\begin{aligned} \mathbf{D}(\mathbf{I}) &= \begin{bmatrix} C_\phi & 0 \\ 0 & C_p \end{bmatrix} \otimes C_s(i) \\ \mathbf{D}(\check{\mathbf{I}}) &= P_{[\bar{e}, \bar{\mu}]}^\perp \begin{bmatrix} C_\phi & 0 \\ 0 & C_p \end{bmatrix} \otimes [C_s(i) - \frac{1}{kn} \bar{C}_s] \end{aligned} \quad (61)$$

Table 5 (Co)Variance matrices of the ambiguity-fixed geometry-free (GF) corrections. The ambiguities, phase and code biases are assumed constant over k epochs.

$Q_{d\hat{d}\hat{d}(i)}^{GF}$	$= \frac{1}{n} Q_{d\hat{d}\hat{d}(i)}^{GF} + \frac{n-1}{n} c_\rho^2 \bar{C}_s + \frac{n-1}{kn^2} \Delta c_\rho^2 \otimes \bar{C}_s$
$Q_{\hat{\delta}\hat{\delta}}^{GF}$	$= \frac{1}{n} Q_{\hat{\delta}\hat{\delta}}^{GF} + \frac{n-1}{kn^2} A^{-1} ([e, -\mu] \Delta Q_{[\hat{\rho}, \hat{e}]} [e, -\mu]^T) A^{-1} \otimes \bar{C}_s$
$Q_{\hat{d}\hat{d}}^{GF}$	$= Q_{\hat{d}\hat{d}}^{GF}$
$Q_{d\hat{\delta}\hat{\delta}(i)}^{GF}$	$= \frac{1}{n} Q_{d\hat{\delta}\hat{\delta}(i)}^{GF} - \frac{n-1}{kn^2} (\Delta c_\rho^2 e^T - \Delta c_{\hat{\rho}\hat{e}} \mu^T) A^{-1} \otimes \bar{C}_s$
$Q_{d\hat{d}\hat{d}(i)}^{GF}$	$= Q_{d\hat{d}\hat{d}(i)}^{GF}$
$Q_{\hat{\delta}\hat{d}}^{GF}$	$= Q_{\hat{\delta}\hat{d}}^{GF}$

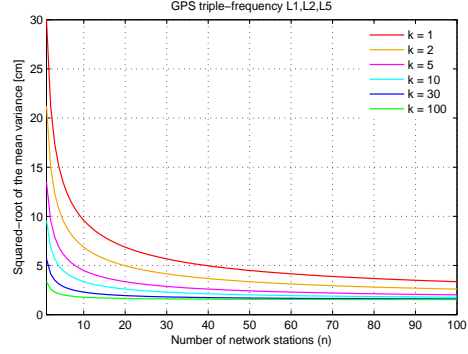


Fig. 2 GPS L1, L2, L5 scenario: the squared-root of the zenith-referenced mean variance of the GF ambiguity-fixed code corrections as a function of the number of stations n for different number of epochs k ($\sigma_\phi = 3$ [mm], $\sigma_p = 30$ [cm], $c_s = 1$).

where $\bar{C}_s^{-1} = \frac{1}{k} \sum_{i=1}^k C_s^{-1}(i)$.

Proof Follows by an application of the variance propagation law to (57). \square

Note that the number of epochs and the number of stations now work in tandem, i.e. they contribute in the same way in improving the precision of the corrections. Figure 2 gives a plot of the square root of the mean variance of an individual satellite at zenith, i.e. $\text{trace}(\mathbf{D}(\check{\tilde{c}}_{p, GF}^s(i)))/f$. Compare the plot with that of Figure 1. In contrast to the ambiguity-float case, the number of stations now has the *same* impact as that of the number of epochs. The impact of the number of stations gets less the larger the number of epochs, and conversely, the impact of the number of epochs gets less the larger the number of stations.

4.5 Relevance of PPP-RTK corrections for user-IAR

As the goal of PPP-RTK is in first instance not so much to improve the *float* solution of the user-position, but rather to enable user integer ambiguity resolution for obtaining a good *ambiguity-fixed* user-position, we revisit the above BLUE corrections (51) and (57), and identify the part that takes an active role in user integer ambiguity resolution. We first consider the network ambiguity-float case and then the network ambiguity-fixed case.

4.5.1 Network ambiguity-float case

Since any part of the corrections that lies in the range space of $\mathcal{P}_{[\bar{e}, \bar{\mu}]}$ gets completely absorbed by the user position and user ionospheric delay parameters, one can discard the part $(\mathcal{P}_{[\bar{e}, \bar{\mu}]} \otimes D_m^T) [\phi_r(\bar{i})^T, p_r(\bar{i})^T]^T$ in (51)

as far as the user-IAR performance is concerned. Hence, for the purpose of user-IAR it then suffices to consider the following simplified corrections

$$\begin{bmatrix} (I_f \otimes D_m^T) \phi_r(\bar{i}) \\ (I_f \otimes D_m^T) p_r(\bar{i}) - (\mathcal{P}_{[e,\mu]}^\perp \otimes D_m^T) p_{\bar{r}r}(\bar{i}) \end{bmatrix} \quad (62)$$

instead of the complete BLUE corrections (51). This shows that only the time-averaged network data is of relevance for user-IAR. Note that this simplified correction even simplifies further in the dual-frequency case, since then $P_{[e,\mu]}^\perp = 0$.

The variance matrix of the above simplified correction (62) is given as

$$\frac{1}{k} \begin{bmatrix} C_\phi & 0 \\ 0 & (I_f - \frac{n-1}{n} \mathcal{P}_{[e,\mu]}^\perp) C_p \end{bmatrix} \otimes \bar{C}_s \quad (63)$$

4.5.2 Network ambiguity-fixed case

In the network ambiguity-fixed case it is the part $(\mathcal{P}_{[\bar{e},\bar{\mu}]} \otimes D_m^T) [[\phi_r(\bar{i}) + \phi_{\bar{r}r}(\bar{i})]^T, [p_r(\bar{i}) + p_{\bar{r}r}(\bar{i})]^T]^T$ in (57) that has no role in user integer ambiguity resolution. Hence, for the purpose of user-IAR it then suffices to consider the following simplified corrections

$$(I_{2f} \otimes D_m^T) \begin{bmatrix} \tilde{\phi}_{\bar{r}}(\bar{i}) \\ p_{\bar{r}}(\bar{i}) \end{bmatrix}, \quad (64)$$

This shows that now, next to the time-averaging, also the station-averaging contributes to the user-IAR. The variance-matrix of (64) reads

$$\frac{1}{kn} \begin{bmatrix} C_\phi & 0 \\ 0 & C_p \end{bmatrix} \otimes \bar{C}_s \quad (65)$$

now clearly showing how k and n work in tandem for improved user-IAR.

4.6 User Ambiguity Dilution of Precision

In this subsection, we use the Ambiguity Dilution of Precision (ADOP) measure (Teunissen, 1997b) to characterize the role of the network's contributing factors, i.e. the number of epochs k and stations n , as well as the role of the number of frequencies f on the strength of user ambiguity resolution. The ADOP is defined as the square-root of the geometric mean of the ambiguity variance matrix's eigenvalues, thus representing the average ambiguity precision. The smaller the ADOP, the larger the ambiguity success rate. As a rule of thumb, ADOP-values smaller than about 0.10 cycle correspond with success rates larger than 0.999 (Odijk and Teunissen, 2008).

The following lemma presents an analytical expressions of the user single-epoch ADOP, once the geometry-free network corrections are applied to the user observations.

Lemma 3 (User single-epoch ADOP: geometry-free network corrections) *Let $C_\phi = \sigma_\phi^2 I_f$ and $C_p = \sigma_p^2 I_f$, respectively, be the co-factor matrices of the network's phase and code observable types in (40), where $C_S(i) \approx \bar{C}_S$. With a likewise structure, let the user phase and code co-factor matrices be given as $C_{\phi_u} = \sigma_{\phi_u}^2 I_f$ and $C_{p_u} = \sigma_{p_u}^2 I_f$, respectively. The user single-epoch ADOP, based on the k -epoch geometry-free network corrections, reads then*

$$\text{ADOP} = c_o \left(\frac{\sigma_{\phi_{u,c}}}{\bar{\lambda}} \right)^{\frac{1}{2}} \left(\frac{\sigma_{p_{u,c}}}{\bar{\lambda}} \right)^{\frac{1}{2}} (1 + \epsilon)^{\frac{1}{2f}} \epsilon^{\frac{f-2}{4f}} \times \left(\frac{1+\epsilon}{\epsilon} + \frac{4\bar{\mu}^2}{(1+\epsilon)\sigma_\mu^2} \right)^{\frac{\nu}{2f(m-1)}} \quad (66)$$

where

$$\sigma_{\phi_{u,c}}^2 = \begin{cases} \sigma_{\phi_u}^2 + \frac{1}{k} \sigma_\diamond^2, & \text{network ambiguity-float} \\ \sigma_{\phi_u}^2 + \frac{1}{kn} \sigma_\diamond^2, & \text{network ambiguity-fixed} \end{cases} \quad (67)$$

with $\diamond = \{\phi, p\}$, $\epsilon = (\sigma_{\phi_{u,c}}^2 / \sigma_{p_{u,c}}^2)$, $\bar{\lambda} = \prod_{j=1}^f \lambda_j^{\frac{1}{f}}$, $\bar{\mu} = (1/f) \sum_{j=1}^f \mu_j$, $\sigma_\mu^2 = (1/f) \sum_{j=1}^f (\mu_j - \bar{\mu})^2$, and

$$c_o = \left(\sum_{s=1}^m c_s^{-2} / \prod_{s=1}^m c_s^{-2} \right)^{\frac{1}{2(m-1)}} \quad (68)$$

with c_s^2 being the diagonal entries of the elevation weighting matrix \bar{C}_S .

Proof Follows from an application of the results of Odijk and Teunissen (2008). \square

The above lemma clearly shows that the number of stations n has *no* role in the user ADOP, when the ambiguity-float network corrections are applied (cf. 67). While in the network ambiguity-float case, the number of epochs k governs the user ADOP, in the network ambiguity-fixed case, both the number of epochs k and stations n work in tandem to reduce the user ADOP. This reduction is, however, bounded by the precision of the user data. For sufficiently large number of epochs and stations, one can *at most* tackle the uncertainty of the network corrections, thereby leaving the precision of the user data to solely govern user ambiguity resolution.

Numerical graphs for the user ADOP, when the ambiguity-fixed network corrections are applied, are given in Figure 3 (solid lines). It shows the ADOP values decrease as both k and n increase. As one would expect, the ADOPs do not get smaller than certain values, because of the nonzero variances of the user data.

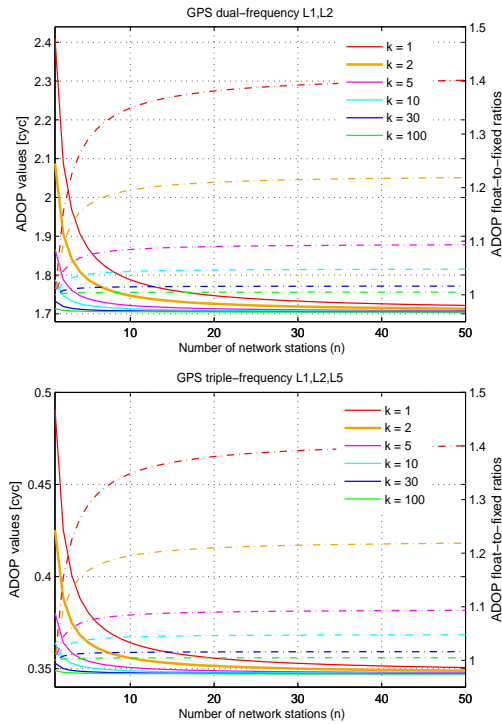


Fig. 3 User single-epoch ADOP values based on the k -epoch geometry-free, ambiguity-fixed network corrections (solid lines) as well as their float-to-fixed ratios (dashed lines) as a function of the number of stations n . *Top*: GPS L1, L2 scenario; *Bottom*: GPS L1, L2, L5 scenario. The values follow from (66) by setting $m = \nu + 1 = 5$, $\sigma_{\phi_u} = \sigma_{\phi} = 3$ [mm], $\sigma_{p_u} = \sigma_p = 30$ [cm], $c_s = 1$.

Next to the ADOP values, Figure 3 also gives the ratio of the ADOP, based on the ambiguity-float network, to the ADOP based on the ambiguity-fixed network (dashed lines). It is observed that these float-to-fixed ratios get larger, the larger the number of stations n . As the number of epochs k increases, their dependency on n gets weaker, though. In the extreme case, when k is large enough, these ratios become all equal to one, meaning that no gain is obtained through replacing the ambiguity-float network corrections by their ambiguity-fixed counterparts.

To show the role of the number of frequencies f on the size of the ADOP, let us first make some approximation. Using $\frac{1+\epsilon}{\epsilon} \approx \frac{1}{\epsilon}$ and neglecting $\frac{4\bar{\mu}^2}{(1+\epsilon)\sigma_{\mu}^2}$ in the last expression of (66), the ADOP is shown to approximately behave as

$$\text{ADOP} \propto \epsilon^{\frac{(f-2)(m-1)-2\nu}{4f(m-1)}} \quad m = \nu + 1 \quad \epsilon^{\frac{f-4}{4f}} \quad (69)$$

where the notation \propto means ‘almost proportional to’. In the absence of satellite redundancy ($m = \nu + 1$), the above quantity decreases from $\epsilon^{-1/4} \approx 10$ ($f = 2$) to $\epsilon^{-1/12} \approx 2.15$ ($f = 3$), where $\epsilon \approx 10^{-4}$. Thus the single-epoch ADOP gets almost 5 times smaller by going from the dual-frequency case to the triple-frequency

Table 6 Extra network redundancy brought by the geometry-based scenario (cf. Table 3).

Scenario	Type	Size
(5) single-epoch ($n > 1$)	$(D_m^T G)^{\perp T} \bar{\rho}$ over n stations	$(m - 1 - \nu)(n - 1)$
(6) multi-epoch ($k > 1, n > 1$)	$(D_m^T G) \Delta X D_n$ over k epochs	$(k - 1)(m - 1)(n - 1)$
# Extra redundancy		$(k[m - 1] - \nu)(n - 1)$

case. This is in agreement with the numerical results given in Figure 3. If the number of satellites m increases however, the stated ADOP reduction becomes smaller. For instance when the number of satellites increases by ν (i.e. $m = 2\nu + 1$), the quantity in (69) decreases from $\epsilon^{-1/8} \approx 3.16$ ($f = 2$) to $\epsilon^0 = 1$ ($f = 3$). In this case, the single-epoch ADOP decreases by almost a factor of 3.

5 Geometry-Based Network Derived Corrections

5.1 Extra redundancy by the geometry-based scenario

So far we based our network analysis on the geometry-free model (39), where information about the relative receiver-satellite geometry was *absent* in its design matrix. We now consider the case where the receiver-satellite geometry is incorporated into the model and study the impact such increase in redundancy brings. The underlying model is referred to as *geometry-based* (GB) (Teunissen, 1997a).

In the following, we show that the k -epoch redundancy of the GB network model is given by

$$\begin{aligned} \# \text{GB redundancy} = \\ \# \text{GF redundancy} + (k[m - 1] - \nu)(n - 1) \end{aligned} \quad (70)$$

A quick overview of the elements building up the above extra redundancy is provided in Table 6.

Recall from (9) that the ν -vectors Δx_r ($r = 1, \dots, n$) of the stations’ position increments/ZTDs are linked, through $\Delta \rho_r^{ps} = g_r^{psT} \Delta x_r$, to the estimable non-dispersive delays $\tilde{\rho}_r^{ps}$. For the sake of presentation, we assume the network to be such that $g_r^{ps} = g^{ps}$, $r = 1 \dots, n$. This assumption admits the inclusion of small to regional networks in our discussion. With this in mind, the DD non-dispersive delays $\Delta \rho_{rl}^{ps} = \tilde{\rho}_l^{ps} - \tilde{\rho}_r^{ps} = \Delta \rho_l^{ps} - \Delta \rho_r^{ps}$ can be further parametrized as

$$\Delta \rho_{rl}^{ps} = g^{psT} (\Delta x_l - \Delta x_r) \quad (71)$$

Table 7 (Co)Variance matrices of the ambiguity-float geometry-based (GB) corrections. The ambiguities, phase and code biases are assumed constant over k epochs.

$Q_{d\hat{d}\hat{d}(i)}^{GB}$	$=$	$Q_{d\hat{d}\hat{d}(i)}^{GF} - \frac{n-1}{n}[\frac{1}{k}c_{\tilde{\rho}}^2\tilde{C}_s + c_{\tilde{\rho}}^2(C_s(i) - \frac{1}{k}\bar{C}_s)]$
$Q_{\hat{\delta}\hat{\delta}}^{GB}$	$=$	$Q_{\hat{\delta}\hat{\delta}}^{GF} - \frac{n-1}{kn}(c_{\tilde{\rho}}^2\Lambda^{-1}e_{\mu}e_{\mu}^T\Lambda^{-1}) \otimes \tilde{C}_s$
$Q_{\hat{d}\hat{d}}^{GB}$	$=$	$Q_{\hat{d}\hat{d}}^{GF}$
$Q_{d\hat{\delta}\hat{\delta}(i)}^{GB}$	$=$	$Q_{d\hat{\delta}\hat{\delta}(i)}^{GF} + \frac{n-1}{kn}(c_{\tilde{\rho}}^2e_{\mu}^T)\Lambda^{-1} \otimes \tilde{C}_s$
$Q_{d\hat{i}\hat{d}}^{GB}$	$=$	$Q_{d\hat{i}\hat{d}}^{GF}$
$Q_{\hat{\delta}\hat{d}}^{GB}$	$=$	$Q_{\hat{\delta}\hat{d}}^{GF}$

$$e_{\mu} = e - \frac{c_{\tilde{\rho}}\hat{i}}{c_{\tilde{\rho}}^2}\mu; \tilde{C}_s = D_m^T \mathcal{P}_{\tilde{G}}^{\perp} \bar{C}_s D_m; \tilde{G} = [e_m, G]$$

or in the multivariate form as

$$\tilde{\rho} D_n = (D_m^T G) \Delta X D_n \quad (72)$$

with $\Delta X = [\Delta x_1, \dots, \Delta x_n]$ and the geometry matrix $G = [g^1, \dots, g^m]^T$.

Equation (72) shows that $(n-1)$ times $(m-1)$ non-dispersive parameters $\tilde{\rho} D_n$ are replaced by $(n-1)$ times ν parameters $\Delta X D_n$, when one switches from the geometry-free model to the geometry-based model. Thus in the single-epoch case, the redundancy increases by $(m-1-\nu)(n-1)$, forming the following condition equations

$$(D_m^T G)^{\perp T} \tilde{\rho} D_n = 0 \quad (73)$$

where $(D_m^T G)^{\perp}$ denotes an orthogonal complement basis matrix of $D_m^T G$ (Teunissen, 2000).

In the k -epoch case, would one assume the relative position increments and ZTDs $(\Delta x_l - \Delta x_r)$ to be time-invariant, all the DD non-dispersive delays $\Delta \rho_{rl}^{ps}(i)$, $i = 2, \dots, k$ (of the second epoch and beyond) are linked to their first-epoch counterparts in (71). This yields an extra redundancy of $(k-1)$ times $(m-1)(n-1)$. Following Teunissen (1997a), if the time-averaged receiver-satellite geometry is used as approximation, the corresponding condition equations can be written as

$$(\tilde{\rho}(i) - \tilde{\rho}(1)) D_n = 0, \quad i = 2, \dots, k \quad (74)$$

Summing the extra redundancies $(m-1-\nu)(n-1)$ and $(k-1)(m-1)(n-1)$ gives (70).

5.2 The Ambiguity-Float GB corrections

Our analytical analysis of the geometry-based, ambiguity-float network-based PPP-RTK corrections are presented in this section. We first derived the BLUE estimators of the individual PPP-RTK corrections $d\tilde{t}^{ps}$, $\tilde{\delta}^{ps}$ and \tilde{d}^{ps} . Their precision is described by the variance-covariance matrices as given in Table 7. The results are linked

to their GF counterparts. It is remarkable that the (co)variance matrices, corresponding to the satellite code biases \tilde{d}^{ps} , remain *unchanged* by switching from the GF-model to the GB-model. Thus the satellite code biases \tilde{d}^{ps} are not only *uncorrelated* with the float DD ambiguities, but also with the relative position increments/ZTDs $(\Delta x_l - \Delta x_r)$. The precision improvement in the satellite clocks and phase biases is governed by matrix $\tilde{C}_s = D_m^T \mathcal{P}_{\tilde{G}}^{\perp} \bar{C}_s D_m$, where $\tilde{G} = [e_m, G]$ (e_m is the m -vector of ones). In the absence of satellite redundancy, we have $m = \nu + 1$ and therefore $\tilde{C}_s = 0$. In that case, the (co)variance matrices, corresponding to the satellite phase biases $\tilde{\delta}^{ps}$, remain unchanged. For the variance matrix of the satellite clocks $d\tilde{t}^{ps}$, there is still a slight improvement, one that can be explained by the assumed time-invariance of $(\Delta x_l - \Delta x_r)$, cf. (74).

Based on the individual corrections we construct the geometry-based, ambiguity-float combined corrections $(\hat{c}_{\phi}^T, \hat{c}_p^T)^T$. First we present their estimators and then their variance-covariance matrices.

Theorem 3 (GB ambiguity-float corrections) *The k -epoch geometry-based ambiguity-float BLUE of the network-derived corrections, at epoch i , is given as*

$$\begin{bmatrix} \hat{c}_{\phi, GB}(i) \\ \hat{c}_{p, GB}(i) \end{bmatrix} = \begin{bmatrix} \hat{c}_{\phi, GF}(i) \\ \hat{c}_{p, GF}(i) \end{bmatrix} - \hat{\mathbb{N}} - \hat{\mathbb{V}} \quad (75)$$

with

$$\hat{\mathbb{N}} = ([\mathcal{P}_{[\bar{e}, \bar{\mu}]} - \mathcal{P}_{\bar{\mu}}] \otimes D_m^T) \begin{bmatrix} \phi_{\bar{r}\bar{r}}(\bar{i}\bar{i}) \\ p_{\bar{r}\bar{r}}(\bar{i}\bar{i}) \end{bmatrix} \quad (76)$$

$$\hat{\mathbb{V}} = \begin{bmatrix} 0 \\ ([\mathcal{P}_{[e, \mu]} - \mathcal{P}_{\mu}] \otimes D_m^T \mathcal{P}_{\tilde{G}}^{\perp}) p_{\bar{r}\bar{r}}(\bar{i}) \end{bmatrix}$$

and the projectors

$$\begin{aligned} \mathcal{P}_{\mu} &= c_{i|\rho}^2 \mu \mu^T C_p^{-1} \\ \mathcal{P}_{\bar{\mu}} &= c_{i|\rho}^2 \tilde{\mu} \tilde{\mu}^T \text{blkdiag}(C_{\phi}^{-1}, C_p^{-1}) \\ \mathcal{P}_{\tilde{G}} &= \tilde{G}(\tilde{G}^T C_S^{-1} \tilde{G})^{-1} \tilde{G}^T C_S^{-1}, \quad \mathcal{P}_{\tilde{G}}^{\perp} = I_m - \mathcal{P}_{\tilde{G}} \end{aligned} \quad (77)$$

where $\tilde{G} = [e_m, G]$, and

$$\begin{aligned} c_{i|\rho}^2 &= (\mu^T C_p^{-1} \mu)^{-1}, \\ c_{i|\rho}^2 &= (\tilde{\mu}^T \text{blkdiag}(C_{\phi}^{-1}, C_p^{-1}) \tilde{\mu})^{-1} \end{aligned} \quad (78)$$

Proof See Appendix. \square

The GB-correction (75) is linked to its GF counterpart (51) through the *zero-mean* terms $\hat{\mathbb{N}}$ and $\hat{\mathbb{V}}$. The first term $\hat{\mathbb{N}}$ describes the contribution of the additional multi-epoch condition equations of (74). Thus $\hat{\mathbb{N}} = 0$ if $\bar{i} = i$. On the other hand, the second term $\hat{\mathbb{V}}$ describes the contribution of the geometry-based condition equations of (73). Thus $\hat{\mathbb{V}}$ vanishes in the absence of satellite

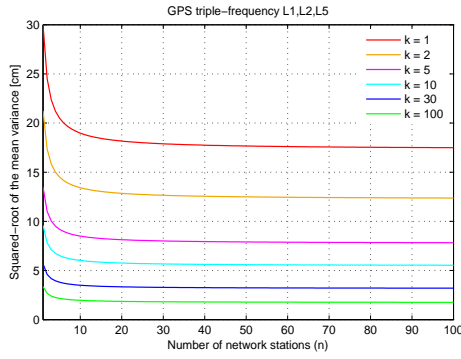


Fig. 4 GPS L1, L2, L5 scenario: the squared-root of the zenith-referenced mean variance of the geometry-fixed, ambiguity-float code corrections as a function of the number of stations n for different number of epochs k ($\sigma_\phi = 3$ [mm], $\sigma_p = 30$ [cm], $c_s = 1$).

redundancy, i.e. $\hat{V} = 0$ if $m = \nu + 1$. Also note that both terms are absent when a single network station is considered, i.e. $\hat{N} = \hat{V} = 0$ if $\bar{r} = r$.

It should be remarked that the third term \hat{V} only contains code data. Hence, in the ambiguity-float case, only the code correction \tilde{c}_p benefits from the contribution of the geometry-based condition equations of (73).

The precision of the above corrections is given in the following lemma.

Lemma 4 (Precision GB ambiguity-float corrections) *The variance matrix of the corrections (75) is given as*

$$\mathbf{D}\left(\begin{bmatrix} \tilde{c}_{\phi,GB}(i) \\ \tilde{c}_{p,GB}(i) \end{bmatrix}\right) = \mathbf{D}\left(\begin{bmatrix} \tilde{c}_{\phi,GF}(i) \\ \tilde{c}_{p,GF}(i) \end{bmatrix}\right) - \mathbf{D}(\hat{N}) - \mathbf{D}(\hat{V}) \quad (79)$$

with

$$\mathbf{D}(\hat{N}) = \frac{n-1}{n} [\mathcal{P}_{[\bar{e},\bar{\mu}]} - \mathcal{P}_{\bar{\mu}}] \begin{bmatrix} C_\phi & 0 \\ 0 & C_p \end{bmatrix} \otimes [C_s(i) - \frac{1}{k} \bar{C}_s] \quad (80)$$

$$\mathbf{D}(\hat{V}) = \frac{n-1}{n} \begin{bmatrix} 0 & 0 \\ 0 & [\mathcal{P}_{[e,\mu]} - \mathcal{P}_\mu] C_p \end{bmatrix} \otimes \frac{1}{k} \tilde{C}_s$$

where $\tilde{C}_s = D_m^T \mathcal{P}_G^\perp \bar{C}_s D_m$.

Proof Follows by an application of the variance propagation law to (75). \square

To evaluate the maximum precision improvement brought by switching to the geometry-based model, we consider the extreme case, namely, the *geometry-fixed* case. The geometry-fixed (GF_i) case refers to the situation where all the relative position increments/ZTDs ($\Delta x_l - \Delta x_r$), $l \neq r$, are assumed known. The GF_i (co)variance matrices follow by setting $\tilde{C}_s = \bar{C}_s$ in (79). Figure 4 gives a plot of the square root of the mean variance of an individual satellite at zenith, i.e. $\text{trace}(\mathbf{D}(\tilde{c}_{p,GB}^s(i)))/f$. Compare the plot with its GF-counterpart in Figure 1.

Table 8 (Co)Variance matrices of the ambiguity-fixed geometry-based (GB) corrections. The ambiguities, phase and code biases are assumed constant over k epochs.

$$\begin{aligned} Q_{d\tilde{t}\tilde{t}(i)}^{GB} &= Q_{d\tilde{t}\tilde{t}(i)}^{GB} - \frac{n-1}{kn} (c_\rho^2 - c_\rho^2) (\bar{C}_s - \tilde{C}_s) \\ Q_{\tilde{\delta}\tilde{\delta}}^{GB} &= Q_{\tilde{\delta}\tilde{\delta}}^{GB} - \frac{n-1}{kn} (c_\rho^2 \Lambda^{-1} e_\mu e_\mu^T \Lambda^{-1}) (\bar{C}_s - \tilde{C}_s) - Q \\ Q_{\tilde{d}\tilde{d}}^{GB} &= Q_{\tilde{d}\tilde{d}}^{GB} \end{aligned}$$

$$\begin{aligned} Q_{d\tilde{\delta}\tilde{\delta}(i)}^{GB} &= Q_{d\tilde{\delta}\tilde{\delta}(i)}^{GB} + \frac{n-1}{kn} (c_\rho^2 e_\mu^T \Lambda^{-1}) (\bar{C}_s - \tilde{C}_s) \\ Q_{d\tilde{t}\tilde{d}}^{GB} &= Q_{d\tilde{t}\tilde{d}}^{GB} \\ Q_{\tilde{\delta}\tilde{d}}^{GB} &= Q_{\tilde{\delta}\tilde{d}}^{GB} \end{aligned}$$

$$Q = \frac{n-1}{kn} \Lambda^{-1} (C_\phi + c_{i|\rho}^2 \mu \mu^T) \Lambda^{-1} \otimes \bar{C}_s$$

The number of stations n now has a *larger* impact on the precision improvement of the code correction. This is mainly due to the extra condition equations of (73) that link the non-dispersive delays $\tilde{\rho}_r^{ps}$ ($r = 1, \dots, n$) to one another. Similar to the GF case however, the stated impact gets less the larger the number of epochs k .

5.3 The Ambiguity-Fixed GB Corrections

We now present our analytical analysis of the geometry-based, ambiguity-fixed network-based PPP-RTK corrections. The precision of the BLUE estimators of the individual PPP-RTK corrections $d\tilde{t}^{ps}$, $\tilde{\delta}^{ps}$ and \tilde{d}^{ps} is described by the variance-covariance matrices as given in Table 8. The ambiguity-fixed results are expressed in their ambiguity-float counterparts. In contrast to the GF-model, here the impact of ambiguity resolution is dependent on the strength of the GB-model. The stronger the model, the lower the impact of ambiguity resolution. The strongest model follows by the geometry-fixed case. In this extreme case, with $\tilde{C}_s = \bar{C}_s$, no precision improvement is realized. On the other hand, the impact of ambiguity resolution gets maximum for the weakest model, i.e. when there is no satellite redundancy ($\tilde{C}_s = 0$ as $m = \nu + 1$).

We now present the geometry-based, ambiguity-fixed combined corrections $(\tilde{c}_\phi^T, \tilde{c}_p^T)^T$.

Theorem 4 (GB ambiguity-fixed corrections) *The k -epoch geometry-based ambiguity-fixed BLUE of the network-derived corrections, at epoch i , is given as*

$$\begin{bmatrix} \tilde{c}_{\phi,GB}(i) \\ \tilde{c}_{p,GB}(i) \end{bmatrix} = \begin{bmatrix} \tilde{c}_{\phi,GF}(i) \\ \tilde{c}_{p,GF}(i) \end{bmatrix} - \hat{N} - \hat{V} \quad (81)$$

with

$$\begin{aligned}\hat{\mathbf{V}} &= ([\mathcal{P}_{[\bar{e}, \bar{\mu}]} - \mathcal{P}_{\bar{\mu}}] \otimes D_m^T) \begin{bmatrix} \phi_{\bar{r}r}(\bar{i}i) \\ p_{\bar{r}r}(\bar{i}i) \end{bmatrix} \\ \check{\mathbf{V}} &= ([\mathcal{P}_{[\bar{e}, \bar{\mu}]} - \mathcal{P}_{\bar{\mu}}] \otimes D_m^T \mathcal{P}_{\bar{G}}^{\perp}) \begin{bmatrix} \tilde{\phi}_{\bar{r}r}(\bar{i}) \\ p_{\bar{r}r}(\bar{i}) \end{bmatrix}\end{aligned}\quad (82)$$

where the ambiguity-fixed phase data are given as

$$\begin{aligned}\tilde{\phi}_r &= \phi_r \\ \tilde{\phi}_l &= \phi_l - [A \otimes L] \check{z}_{rl}, \quad l \neq r\end{aligned}\quad (83)$$

with L being an $m \times (m-1)$ matrix formed by removing the p^{th} column of I_m (given p as the pivot satellite).

Proof See Appendix. \square

The GB ambiguity-fixed correction (81) is linked to its GF-counterpart (57) through the *zero-mean* terms $\hat{\mathbf{V}}$ and $\check{\mathbf{V}}$. Compare the results with those of the GB ambiguity-float (75). The first term $\hat{\mathbf{V}}$, due to the multi-epoch condition equations of (74), remains unchanged. This is what one would expect, since the *epoch-differenced* observations $\phi_{\bar{r}r}(\bar{i}i)$ and $p_{\bar{r}r}(\bar{i}i)$ are uncorrelated with the float ambiguities. The second term $\check{\mathbf{V}}$ is, however, replaced by its ambiguity-fixed counterpart $\check{\mathbf{V}}$, describing the contribution of the geometry-based condition equations of (73). Next to the code data, the ambiguity-fixed carrier phase data $\tilde{\phi}_l$ also contribute in a likewise manner to $\check{\mathbf{V}}$.

An application of the variance propagation law to the above corrections gives their precision as presented in the following lemma.

Lemma 5 (Precision GB ambiguity-fixed corrections) *The variance matrix of the corrections (81) is given as*

$$D\left(\begin{bmatrix} \check{c}_{\phi, GB}(i) \\ \check{c}_{p, GB}(i) \end{bmatrix}\right) = D\left(\begin{bmatrix} \check{c}_{\phi, GF}(i) \\ \check{c}_{p, GF}(i) \end{bmatrix}\right) - D(\hat{\mathbf{V}}) - D(\check{\mathbf{V}}) \quad (84)$$

with

$$\begin{aligned}D(\hat{\mathbf{V}}) &= \frac{n-1}{n} [\mathcal{P}_{[\bar{e}, \bar{\mu}]} - \mathcal{P}_{\bar{\mu}}] \begin{bmatrix} C_{\phi} & 0 \\ 0 & C_p \end{bmatrix} \otimes [C_s(i) - \frac{1}{k} \bar{C}_s] \\ D(\check{\mathbf{V}}) &= \frac{n-1}{n} [\mathcal{P}_{[\bar{e}, \bar{\mu}]} - \mathcal{P}_{\bar{\mu}}] \begin{bmatrix} C_{\phi} & 0 \\ 0 & C_p \end{bmatrix} \otimes \frac{1}{k} \tilde{C}_s\end{aligned}\quad (85)$$

Proof Follows by an application of the variance propagation law to (81). \square

We again consider the extreme case, the geometry-fixed case, to evaluate the maximum precision improvement brought by switching to the geometry-based model. The stated improvement follows by setting $\tilde{C}_s = \bar{C}_s$ in (84). A plot of the square root of the mean variance of an individual satellite at zenith, i.e. $\text{trace}(D(\check{c}_{p, GB}^s(i)))/f$,

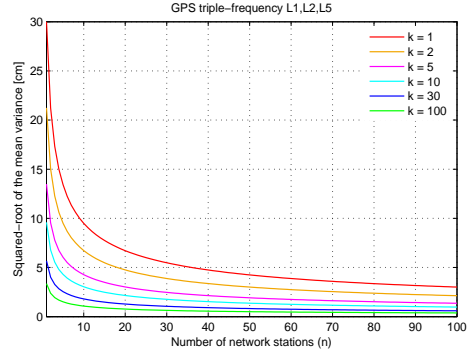


Fig. 5 GPS L1, L2, L5 scenario: the squared-root of the zenith-referenced mean variance of the geometry-fixed, ambiguity-fixed code corrections as a function of the number of stations n for different number of epochs k ($\sigma_{\phi} = 3$ [mm], $\sigma_p = 30$ [cm], $c_s = 1$).

is given in Figure 5. Compare the plot with its GF-counterpart in Figure 2. The precision improvement is indeed insignificant. Provided that successful network ambiguity resolution is applied, one should therefore not expect a considerable improvement in the precision of the corrections, by switching to the geometry-based model. Once the network's ambiguities are resolved, the GF and GB performances do not differ by much.

5.4 User ADOP improvement by the GB corrections

To evaluate how much switching to the geometry-based model pays off, we again consider the user ADOP to characterize the improvement in the strength of user ambiguity resolution. Since adopting the geometry-based scenario further strengthens the network model, one would expect the user ADOP to get smaller upon replacing the geometry-free corrections by the geometry-based corrections. The maximum reduction in the ADOP follows when the geometry-fixed case is considered. The stated reduction is formulated in the following lemma presenting the user single-epoch ADOP GF-to-GFi ratios.

Lemma 6 (User single-epoch ADOP ratio: from geometry-free to geometry-based network corrections) *Let $C_{\phi} = \sigma_{\phi}^2 I_f$ and $C_p = \sigma_p^2 I_f$, respectively, be the co-factor matrices of the network's phase and code observable types in (40), where $C_s(i) \approx \bar{C}_s$. With a likewise structure, let the user phase and code co-factor matrices be given as $C_{\phi_u} = \sigma_{\phi_u}^2 I_f$ and $C_{p_u} = \sigma_{p_u}^2 I_f$, respectively. The ratio of the user single-epoch ADOP, based on the*

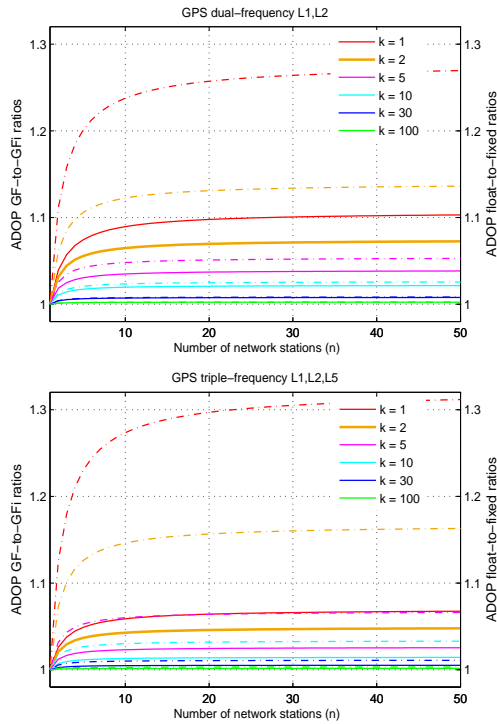


Fig. 6 User ADOP GF-to-GFi ratios (86) of the ambiguity-float network corrections (solid lines) as well as the ADOP float-to-fixed ratios of the GFi network corrections (dashed lines) as a function of the number of stations n . *Top*: GPS L1, L2 scenario; *Bottom*: GPS L1, L2, L5 scenario. The values follow from (86) by setting $m = \nu + 1 = 5$, $\sigma_{\phi_u} = \sigma_{\phi} = 3$ [mm], $\sigma_{p_u} = \sigma_p = 30$ [cm], $c_s = 1$.

k -epoch geometry-free network corrections (ADOP_{GF}), to its geometry-fixed counterpart (ADOP_{GFi}) reads then

$$\frac{\text{ADOP}_{\text{GF}}}{\text{ADOP}_{\text{GFi}}} = \begin{cases} \left(\frac{[1+k\gamma_u][1+kn\gamma_u]+k(n-1)\gamma_u}{[1+k\gamma_u][1+kn\gamma_u]+\tilde{\epsilon}k(n-1)\gamma_u} \right)^{\frac{\nu}{2f(m-1)}}, & \text{net. amb.-float} \\ 1 & \text{net. amb.-fixed} \end{cases} \quad (86)$$

with $\gamma_u = (\sigma_{p_u}^2 / \sigma_p^2)$, and

$$\tilde{\epsilon} = \frac{\epsilon}{(1 + \epsilon) + \frac{4\epsilon\bar{\mu}^2}{(1+\epsilon)\sigma_{\mu}^2}} \quad (87)$$

Proof Follows from an application of the results of Odijk and Teunissen (2008). \square

The above lemma conveys two important messages. First, after successful network ambiguity resolution, no matter whether the user is provided with the geometry-free corrections or with the geometry-based corrections, in either case, the user ADOP remains the *same* (i.e. $\text{ADOP}_{\text{GF}} = \text{ADOP}_{\text{GFi}}$).

Second, when the network ambiguity-float scenario is considered, there is a slight reduction in the user ADOP by switching from the geometry-free to the geometry-based corrections. To gain insight into the size

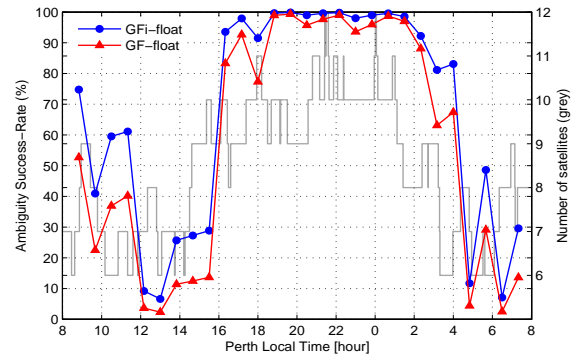


Fig. 7 User ambiguity success-rates (%) based on 28 observational groups (each of size 100 epochs) that are corrected by the single-epoch geometry-fixed (GFi) (blue circles) and geometry-free (GF) ambiguity-float (red triangles) corrections. The number of stations is assumed to be very large, i.e. $n \rightarrow \infty$. The number of visible satellites are depicted by the grey lines (GPS L1, L2 scenario: $\sigma_{\phi_u} = \sigma_{\phi} = 3$ [mm], $\sigma_{p_u} = \sigma_p = 30$ [cm], $\nu = 4$, sampling-interval = 30 seconds). The ambiguity success-rates have been computed using the VISUAL software (Verhagen, 2002).

of this reduction, we make some approximation. Note that one can neglect $\tilde{\epsilon}k(n-1)\gamma_u$, compared to the first term in the denominator of (86). Assuming the user's data to be of the same quality as those of the network receivers (i.e. $\gamma_u = 1$), the first expression of (86) would then takes the following form ($k = 1$)

$$\frac{\text{ADOP}_{\text{GF}}}{\text{ADOP}_{\text{GFi}}} \approx \left[1 + \frac{n-1}{2(n+1)} \right]^{\frac{\nu}{2f(m-1)}} \quad (88)$$

In the absence of satellite redundancy ($m = \nu + 1$), the above ADOP GF-to-GFi ratio becomes around 1.10 (when $f = 2$) and 1.07 (when $f = 3$), would the number of network stations be $n = 100$. When the number of satellites increases by ν (i.e. $m = 2\nu + 1$), the above ADOP GF-to-GFi ratio even gets smaller, around 1.05 ($f = 2$) and 1.03 ($f = 3$). In either case, the stated ratio is therefore close to one, meaning that only a slight improvement in the strength of user ambiguity resolution is realized through replacing the ambiguity-float, geometry-free corrections by their geometry-based counterparts. This analysis is consistent with the numerical results that are shown in Figure 6 (solid lines) for the user-ADOP GF-to-GFi ratios, for the dual- and triple frequency case and different number of epochs k and stations n . This is further corroborated by the user ambiguity success-rates as shown in Figure 7, based on the GFi (blue circles) and the GF ambiguity-float (red triangles) corrections. In order to consider the maximum gain in the user-IAR capacity achieved by switching to the GB model, we consider the dual-frequency single-epoch network corrections ($f = 2$, $k = 1$) where the number of stations is assumed to be very large (i.e.

$n \rightarrow \infty$). The user corrected data have been partitioned into 28 groups, each of size 100 epochs with the sampling-interval of 30 seconds. As predicted by the ADOP analysis, Figure 7 confirms that the user ambiguity success-rates based on the GF corrections do not differ too much from their GF_i versions.

Although switching from the ambiguity-float, geometry-free network scenario to its geometry-based counterpart does not improve the capacity of user ambiguity resolution by much, one must, however, note that it does play a prominent role in improving the capacity of network ambiguity resolution (Teunissen and Khodabandeh, 2015). Furthermore, such a GF-to-GB network switch also improves the float solution of the user position/ZTD, as the clock corrections approximately improve from a 1-over- k rule to a 1-over- kn rule (cf. Table 7 for $\tilde{C}_s = \bar{C}_s$).

Next to the network ambiguity-float, GF-to-GB switch, we also consider the effect of network ambiguity fixing. To compare the user-ambiguity impact of the ambiguity-fixed network corrections with their ambiguity-float counterparts, the user-ADOP float-to-fixed ratios (dashed lines) are shown in Figure 6 for a GF_i-network. The float-to-fixed ratio (dashed lines) is around 1.27 (when $f = 2$) and 1.31 (when $f = 3$) for $k = 1$. When the k -epoch network corrections are applied, the stated ratio does even get smaller as the number of epochs k increases. For instance, the float-to-fixed ratio drops to 1.05 ($f = 2$) and 1.07 ($f = 3$) for $k = 5$.

From the above one may conclude that user ambiguity resolution performance, when based on the PPP-RTK corrections \hat{d}^s , δ^s , and \tilde{d}^s , will not benefit too much from ambiguity fixing in the network. This does not mean, of course, that network ambiguity resolution has no important role to play. It plays a significant role, for instance, in improving the precision of the estimated ionospheric delays in the network (Teunissen and Khodabandeh, 2014).

The reason for the rather modest impact of network ambiguity resolution on the user ambiguity resolution performance lies in the way the user's ionospheric delays are treated. In our formulation, the user's ionospheric delays are treated as unknown, thus resulting in a rather weak model in terms of ambiguity resolution capability. But as was already pointed out in Sect. 2.3.1, one can improve user ambiguity resolution performance significantly if the PPP-RTK corrections would be extended with an ionospheric component, thus enabling the user to make use of the stronger ionosphere-weighted model. In that case, network ambiguity resolution would improve the provided ionospheric information (Odijk, 2002; Grejner-Brzezinska et al, 2004; Mervart et al, 2013; Odijk et al, 2014).

5.5 Corrections' precision relevant to user-IAR

As stated earlier in Sect. 4.5, not all the components of the PPP-RTK corrections contribute to user integer ambiguity resolution. Any part of the corrections that lies in the range space of $\mathcal{P}_{[\bar{e}, \bar{\mu}]}$ gets fully absorbed by the user position and user ionospheric delay parameters, thus not affecting the estimator of the user ambiguities. This in turn allows one to identify which part of the variance matrix of the corrections is relevant to user-IAR, see e.g. (63) and (65). Drawing a similar analogy to the geometry-free network corrections, the following part of the geometry-based network corrections, relevant to user-IAR, can be considered,

network ambiguity-float case:

$$\begin{bmatrix} (I_f \otimes D_m^T) \phi_r(\bar{i}) \\ (I_f \otimes D_m^T) p_r(\bar{i}) - (\mathcal{P}_{[e, \mu]}^\perp \otimes D_m^T) p_{rr}(\bar{i}) - ((\mathcal{P}_{[e, \mu]} - \mathcal{P}_\mu) \otimes D_m^T \mathcal{P}_G^\perp) p_{rr}(\bar{i}) \end{bmatrix} \quad (89)$$

network ambiguity-fixed case:

$$(I_{2f} \otimes D_m^T) \begin{bmatrix} \tilde{\phi}_r(\bar{i}) \\ p_r(\bar{i}) \end{bmatrix} \quad (90)$$

Compare the above equations with their GF counterparts (62) and (64). This again shows that only the time-averaged network data is of relevance for user-IAR. While the GB ambiguity-fixed part (90) is *identical* to that of the GF ambiguity-fixed case (64), the GB ambiguity-float part (89) differs from its GF version (62). This is due to the difference in their *code* corrections only. The stated code-difference is formed by the projector $\mathcal{P}_{[e, \mu]} - \mathcal{P}_\mu$. For the dual-frequency case (i.e. for $\mathcal{P}_{[e, \mu]} = I_f$), this projector is simplified as $\mathcal{P}_{[e, \mu]} - \mathcal{P}_\mu = \mathcal{P}_\mu^\perp$. The projector \mathcal{P}_μ^\perp is referred to as the *ionosphere-free* projector, since it nullifies the ionospheric vector μ , i.e. $\mathcal{P}_\mu^\perp \mu = 0$. Thus in the dual-frequency case, the network ambiguity-float GF-to-GB switch only leads the ionosphere-free code data to contribute to a further improvement of the relevant GF corrections.

The corresponding variance matrices of (89) and (90) are, respectively, given as,

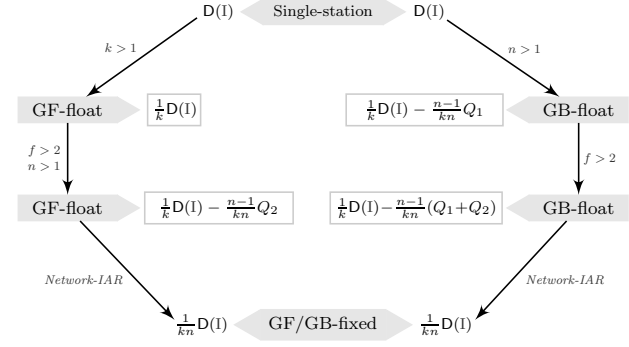
network ambiguity-float case:

$$\frac{1}{k} \begin{bmatrix} C_\phi & 0 \\ 0 & (I_f - \frac{n-1}{n} \mathcal{P}_{[e, \mu]}^\perp) C_p \end{bmatrix} \otimes \bar{C}_s - \frac{n-1}{kn} \begin{bmatrix} 0 & 0 \\ 0 & [\mathcal{P}_{[e, \mu]} - \mathcal{P}_\mu] C_p \end{bmatrix} \otimes \bar{C}_s \quad (91)$$

network ambiguity-fixed case:

$$\frac{1}{kn} \begin{bmatrix} C_\phi & 0 \\ 0 & C_p \end{bmatrix} \otimes \bar{C}_s \quad (92)$$

where an overview of the interactions of the above (co)-variance components with their single-station and geometry-free counterparts is presented by the diagram given in Figure 8. To highlight the role of the number of



$$D(I) = \begin{bmatrix} C_\phi & 0 \\ 0 & C_p \end{bmatrix} \otimes C_s; \quad Q_1 = \begin{bmatrix} 0 & 0 \\ 0 & [\mathcal{P}_{[e,\mu]} - \mathcal{P}_\mu] C_p \end{bmatrix} \otimes \tilde{C}_s; \quad Q_2 = \begin{bmatrix} 0 & 0 \\ 0 & \mathcal{P}_{[e,\mu]}^\perp C_p \end{bmatrix} \otimes C_s$$

Fig. 8 Diagram linking the parts of the network corrections' variance matrices that determine user ambiguity resolution. With the approximation $C_s(i) = C_s$, $i = 1, \dots, k$, the role of the number of epochs k and stations n is characterized by switching from the single-station scenario to the GF- and GB-network scenarios.

epochs k , we make the approximation $C_s(i) = C_s$, $i = 1, \dots, k$. The diagram commences with the variance matrix of the single-station corrections, i.e. $D(I)$ (cf. 56). In case of the multi-epoch scenario ($k > 1$), the relevant part of the variance matrix decreases by a factor of k which is identical to that of the dual-frequency GF ambiguity-float (GF-float) model (cf. 63 for $f = 2$). When the multi-frequency GF-float network scenario takes place (i.e. $n > 1$ and $f > 2$), the stated part is reduced further by $[(n-1)/(kn)]Q_2$ (cf. 63). Note that this reduction vanishes when $n = 1$ or when $f = 2$.

On the other side of the diagram, the link between the single-station variance matrix and the GB ambiguity-float (GB-float) variance matrix is considered (cf. 91 for $f = 2$). At least two network stations are needed to realize the GB-float scenario (i.e. $n > 1$). In contrast to the GF-float model, a *single-epoch* reduction ($k = 1$) in the relevant variance matrix can be achieved upon switching to the GB-float model. The stated single-epoch reduction, for the dual-frequency case, is equal to $[(n-1)/n]Q_1$ that is attributed to the contribution of the ionosphere-free code data (cf. 89). Note that this reduction vanishes when $n = 1$ or when $m = \nu + 1$. In case of the multi-epoch scenario ($k > 1$), the reduced variance matrix decreases by a factor of k . Similar to the GF-float model, going from the dual-frequency case to the multi-frequency case ($f > 2$) reduces the GB variance matrix further by $[(n-1)/(kn)]Q_2$ (cf. 91).

After successful network ambiguity resolution, *both* the GF and the GB variance matrices, relevant to user-IAR, get *identical* to $(1/kn)D(I)$ (cf. 65 and 92). In this case, both the number of epochs k and stations n work in tandem to reduce the relevant variance matrix.

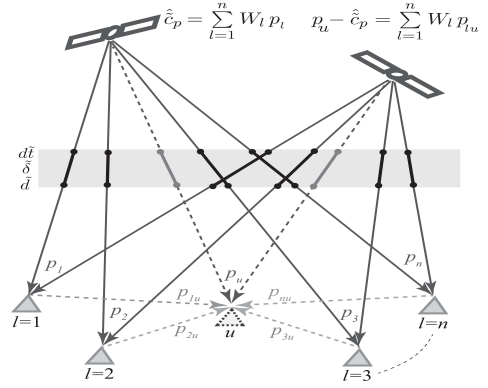


Fig. 9 Illustration of the user corrected observations as a weighted-average of the DD observations formed between the user 'u' and the network stations $l = 1, \dots, n$.

5.6 User corrected data interpreted as DD data

In Sect. 2, an analogy between the single-station PPP-RTK setup and the single-baseline RTK setup was given (cf. Table 1). It was shown that the user corrected data are nothing else but DD observations formed between the user and a single network station. This is the case as the single-station corrections stand in one-to-one correspondence with the single-station observations (cf. 17). On the other hand, through the presentation of Theorems 1–4, the PPP-RTK network corrections were shown to be an *adjusted* version of single-station observations. It is therefore evident that the user's corrected observations, on the basis of the *network* corrections, can also be interpreted as DD observations between the user and the network stations. This notion is visualized in Figure 9 and made precise via the following theorem.

Theorem 5 (PPP-RTK in DD-form) *Let $[\phi_u^T(i), p_u^T(i)]^T$ be the user observations at epoch i . Also let the k -epoch network correction $[\hat{c}_\phi^T(i), \hat{c}_p^T(i)]^T$ be a linear unbiased estimator of $[\tilde{c}_\phi^T(i), \tilde{c}_p^T(i)]^T$. Then the user corrected observations can always be written as*

$$\begin{bmatrix} (I_f \otimes D_m^T) \phi_u(i) \\ (I_f \otimes D_m^T) p_u(i) \end{bmatrix} - \begin{bmatrix} \hat{c}_\phi(i) \\ \hat{c}_p(i) \end{bmatrix} = \sum_{q=1}^k \sum_{l=1}^n W_{q,l}(i) \begin{bmatrix} (I_f \otimes D_m^T) \phi_{lu}(q) \\ (I_f \otimes D_m^T) p_{lu}(q) \end{bmatrix} \quad (93)$$

for some weight matrices $W_{q,l}(i)$ satisfying

$$\sum_{q=1}^k \sum_{l=1}^n W_{q,l}(i) = I \quad (94)$$

with the DD observations

$$\begin{aligned} (I_f \otimes D_m^T) \phi_{lu}(q) &= (I_f \otimes D_m^T) [\phi_u(i) - \phi_l(q)] \\ (I_f \otimes D_m^T) p_{lu}(q) &= (I_f \otimes D_m^T) [p_u(i) - p_l(q)] \end{aligned}$$

Proof Follows by an application of Theorems 1–4. \square

According to the above theorem, the user corrected observations can always be viewed as a *weighted-average* of DD observations formed between the user and the network stations. To give an example, consider the user-corrected code observable based on the single-epoch GF-float corrections (i.e. $\hat{\mathbb{I}} = 0$ in 51). For one single element of the code correction we may write then

$$\begin{aligned}\hat{c}_{p,GF}^{ps} &= \mathcal{P}_{[e,\mu]} p_{rr}^{ps} + p_{\bar{r}}^{ps} \\ &= \mathcal{P}_{[e,\mu]} p_r^{ps} + \mathcal{P}_{[e,\mu]}^\perp p_{\bar{r}}^{ps}\end{aligned}\quad (95)$$

thus forming the user corrected code observations as

$$p_u^{ps} - \hat{c}_{p,GF}^{ps} = \mathcal{P}_{[e,\mu]} p_{ru}^{ps} + \mathcal{P}_{[e,\mu]}^\perp \frac{1}{n} \sum_{l=1}^n p_{lu}^{ps}\quad (96)$$

with the DD observations $p_{lu}^{ps} = p_u^{ps} - p_l^{ps}$. Equation (96) can then be expressed as a weighted-average of p_{lu}^{ps} , $l = 1, \dots, n$, that is

$$p_u^{ps} - \hat{c}_{p,GF}^{ps} = \sum_{l=1}^n W_l p_{lu}^{ps}, \quad \text{with} \quad \sum_{l=1}^n W_l = I\quad (97)$$

in which the weight matrices W_l are defined as

$$W_l = \begin{cases} \mathcal{P}_{[e,\mu]} + \frac{1}{n} \mathcal{P}_{[e,\mu]}^\perp, & l = r \\ \frac{1}{n} \mathcal{P}_{[e,\mu]}^\perp, & l \neq r \end{cases}\quad (98)$$

It therefore follows from the *DD-like* structure of the PPP-RTK user corrected observations that the PPP-RTK setup can be considered equivalent to the more traditional network-RTK setup, be it that their ionospheric parametrization could be different.

6 Summary and conclusions

The contributions of this paper are summarized as follows:

- *Single-station PPP-RTK*: It was shown how a proper set of estimable parameters of a *single station* can act as if they are the satellite clocks and phase/code biases, respectively. In their application to the user observation equations, we characterized the role of each such PPP-RTK correction. The estimable satellite clock $\tilde{d}\hat{t}$ provides a ‘positional link’ between the user and reference station, while the estimable satellite phase biases $\tilde{\delta}$ have the function of replacing the noninteger user ambiguity by the integer double-differenced (DD) ambiguity between the user and the reference station. It was also shown that for the *multi-frequency* PPP-RTK setup one needs the additional code bias correction \tilde{d} , so as to make optimal use of the user code data on the third frequency and beyond ($f > 2$).

- *Highly correlated PPP-RTK corrections*: It was shown that one should not rely on the quality-judgment of the individual corrections. Instead, the quality of the *combined* version of the corrections must be evaluated. This is because of the high correlation that exists between the individual corrections. By means of some illustrative examples we demonstrated the potential pitfalls of ignoring the stated correlation.
- *Single-station PPP-RTK is single-baseline RTK*: We demonstrated the equivalence between the single-station PPP-RTK setup and the more traditional single-baseline RTK setup (cf. Table 1). It was shown that both formulations are identical except for their ionospheric delay parameters. With the PPP-RTK user model a biased ionospheric delay is obtained, whereas an unbiased DD ionospheric delay is obtained with the single-baseline model.
- *Network redundancy for PPP-RTK*: We identified the network redundancy and its impact on the precision of the PPP-RTK corrections (cf. Tables 3 and 6). This was done for both the geometry-free (GF) network model and the geometry-based (GB) network model, with and without network-IAR. The precision impact of the number of epochs k , number of stations n and number of frequencies f was shown for both the individual corrections as well as for their combined form. Furthermore it was demonstrated that the estimable code biases are *uncorrelated* with the float DD ambiguities and the stations’ relative positions/ZTDs. Hence, their (co)variance matrices remain *unchanged* when switching to the geometry-based model and/or when performing integer ambiguity resolution.
- *BLUES of PPP-RTK corrections*: We derived the best linear unbiased estimators of the PPP-RTK network corrections in analytical form. The BLUES of the combined corrections are expressed in terms of time- and station-*averaged* network observations and time- and station-*differenced* network observations. By using the conditional least-squares approach, our result is formulated such that it clearly shows how the single-station corrections are further improved by the network information. Therefore once the corrections are applied to the user data, the user corrected observation equations can be interpreted as if a single baseline is formed between the user and a network-adjusted reference station.
- *Only time-averaged network data relevant for user-IAR*: The closed-form expressions of the BLUE corrections allow one to identify which part of the combined corrections really contributes to user integer ambiguity resolution. For all four network scenarios (i.e. the GF-float, cf. 62, the GF-fixed, cf. 64,

Table 9 Precision impact of the network corrections on the user float ambiguities and on the float position/ZTD for the geometry-free (GF) and the geometry-fixed (GF_i) network scenarios. With the approximation $C_s(i) = C_s$, $i = 1, \dots, k$, the role of the number of epochs k is highlighted. The variance matrices $D(I)$, Q_1 and Q_2 are given in Figure 8. The $f \times (f - 1)$ matrix B is a basis matrix orthogonal-complement to the f -vector μ , thus forming ionosphere-free combinations.

Scenario	Variance matrix relevant to the user-ambiguities		Variance matrix relevant to the user-float position/ZTD	
	Net. ambiguity-float	Net. ambiguity-fixed	Net. ambiguity-float	Net. ambiguity-fixed
GF:	$Q_{\text{float}}^{\text{GF}} = \frac{1}{k}D(I) - \frac{n-1}{kn}Q_2$,	$Q_{\text{fixed}}^{\text{GF}} = \frac{1}{n}Q_{\text{float}}^{\text{GF}}$	$Q_{\text{float}}^{\text{GF}} = \frac{1}{k}(c_\rho^2 + [k-1]c_\rho^2)Q_e + \Delta Q$,	$Q_{\text{fixed}}^{\text{GF}} = Q_{\text{float}}^{\text{GF}} + \frac{n-1}{n}c_\rho^2 Q_e$
GF _i :	$Q_{\text{float}}^{\text{GF}_i} = Q_{\text{float}}^{\text{GF}} - \frac{n-1}{kn}(Q_1 + Q_2)$,	$Q_{\text{fixed}}^{\text{GF}_i} = Q_{\text{fixed}}^{\text{GF}}$	$Q_{\text{float}}^{\text{GF}_i} = \frac{1}{n}Q_{\text{float}}^{\text{GF}} + \frac{n-1}{n}\Delta Q$,	$Q_{\text{fixed}}^{\text{GF}_i} = Q_{\text{float}}^{\text{GF}_i}$

$$Q_e = (B^T e e^T B \otimes C_s); \quad \Delta Q = Q_{\hat{\rho}\hat{\rho}} Q_{\hat{d}\hat{d}}^{-1} Q_{\hat{\rho}\hat{d}}^T; \quad Q_{\hat{\rho}\hat{\rho}} = (1/kn)(B^T C_p E^{-T} \otimes C_s); \quad Q_{\hat{d}\hat{d}} = (1/kn)(E^{-T} C_p E^{-T} \otimes C_s)$$

the GB-float, cf. 89, and the GB-fixed, cf. 90) it was shown that the network contribution to the float-estimated user-ambiguities is only through the time-averaged network data. For the two ambiguity-fixed network scenarios (i.e. GF- and GB-fixed, cf. 64 and 90), the network contribution to the float-estimated user-ambiguities becomes even confined to the station-average of the time-averaged network data.

- *Precision impact on user-float position/ZTD:* The GF-to-GB network switch can improve the float solution of the user position/ZTD. This improvement however, largely depends on the geometrical strength of the GB-model and on whether or not network-IAR is applied. The geometrically stronger the model, the larger the precision improvement becomes. In the strongest case, namely, the geometry-fixed (GF_i) case, the precision of the user float position/ZTD, based on the network ambiguity-float corrections, is already as good as that of its network ambiguity-fixed counterpart. In the weakest case, namely, the geometry-free case, the stated precision can almost reach that of the GF_i case, would network-IAR be applied (cf. Table 9). Hence, for the variance matrix of the float solution of the user position/ZTD, the network corrections can be ordered as

$$\text{GF-float} \geq \text{GF-fixed} \approx \text{GF}_i\text{-float} = \text{GF}_i\text{-fixed}$$

- *Precision impact on user-ambiguities:* In the sense of being able to estimate a more precise user ambiguity, the network corrections of the GB ambiguity-float model outperform their GF ambiguity-float counterpart. For their network ambiguity-fixed versions the situation is different. After performing network-IAR, the user-ambiguity relevant parts of both the GB- and GF-based corrections become *identical*, where now both the number of epochs k and the number of stations n work in tandem to improve the user-ambiguity precision (cf. Table 9). Hence, for the variance matrix of the user-ambiguities, the network corrections can be ordered as

$$\text{GF-float} \geq \text{GB-float} \geq \text{GF-fixed} = \text{GB-fixed}$$

- *Relevance of ionospheric information:* Through our user-ADOP analysis the above improvements were also quantified. It was shown that they are not as significant as would be the case when the user would be able to include ionosphere-weighting in his model. This underlines the importance of being able to include network-based ionospheric information in the corrections, an addition that would then benefit most from using the geometry-based, ambiguity-fixed network model. Without such corrections, the user performance corresponds to that of a long baseline ionosphere float model.
- *PPP-RTK user-parameters are function of DD data:* It was shown that the PPP-RTK user corrected data can always be viewed as a *weighted-average* of the double-differenced (DD) observations that are formed between the user and the network stations. This shows the equivalence between the PPP-RTK formulation and the more traditional network-RTK formulation, be it that their ionospheric parametrizations could be different.
- *Network can at most overcome half the uncertainty of the reference-user data:* Recall that the user corrected model of observation equations can be interpreted as being that of a single baseline formed between the user and network-adjusted reference station. Strengthening the network model would therefore only improve the quality of the reference station's data (i.e. the network corrections), which in the extreme case of perfectly known (i.e. non-random) corrections, would still leave the uncertainty of the user data to drive the user positioning performance.

Acknowledgements This work has been done in the context of the Positioning Program Project 1.19 “Multi-GNSS PPP-RTK Network Processing” of the Cooperative Research Centre for Spatial Information (CRC-SI). The second author is the recipient of an Australian Research Council (ARC) Federation Fellowship (project number FF0883188). All this support is gratefully acknowledged.

Appendix

Proof of Theorem 1 To prove (51), we apply the least-squares conditional adjustment (Teunissen, 2000) to the single-station correction ‘I’. Given the GF ambiguity-float network redundancy (Table 3), the following *uncorrelated* sets of misclosures are formed

$$t = (I_{n-1} \otimes E^- \otimes D_m^T) [p_{12}^T(\bar{i}), \dots, p_{1n}^T(\bar{i})]^T, \\ t_l = (I_{k-1} \otimes \begin{bmatrix} A^{-1}, & M \\ 0, & E^- \end{bmatrix} \otimes D_m^T) \begin{bmatrix} \phi_l(12) \\ p_l(12) \end{bmatrix}^T, \dots, \begin{bmatrix} \phi_l(1k) \\ p_l(1k) \end{bmatrix}^T \quad (99)$$

$l = 1, \dots, n$. The first set of misclosures t is due to the fact that all single-station solutions of the estimable code biases \tilde{d}^{ps} have the same mean. The n sets of misclosures t_l are due to the fact that all single-station solutions of the estimable ambiguities \tilde{a}_l^{ps} and code biases \tilde{d}^{ps} are assumed *constant* over k epochs. According to the least-squares conditional adjustment, the GF ambiguity-float network correction (51) is obtained as

$$\begin{bmatrix} \hat{\tilde{c}}_{\phi, GF}(i) \\ \hat{\tilde{c}}_{p, GF}(i) \end{bmatrix} = I - Q_{I,t} Q_{tt}^{-1} t - \sum_{l=1}^n Q_{I,t_l} Q_{t_l t_l}^{-1} t_l \quad (100)$$

This, together with the following equalities

$$Q_{I,t} Q_{tt}^{-1} t = \hat{\mathbb{I}}, \quad \text{and} \quad Q_{I,t_l} Q_{t_l t_l}^{-1} t_l = \begin{cases} \hat{\mathbb{I}}, & l = r \\ 0, & l \neq r \end{cases} \quad (101)$$

completes the proof. \square

Proof of Theorem 2 The proof goes along the same lines as the proof of Theorem 1. The GF ambiguity-fixed network correction (57) is obtained through replacing the role of the misclosure vector t in (100) by its higher-dimension counterpart (cf. Table 3)

$$\bar{i} = (I_{n-1} \otimes \begin{bmatrix} A^{-1}, & M \\ 0, & E^- \end{bmatrix} \otimes D_m^T) \begin{bmatrix} \tilde{\phi}_{12}(\bar{i}) \\ p_{12}(\bar{i}) \end{bmatrix}^T, \dots, \begin{bmatrix} \tilde{\phi}_{1n}(\bar{i}) \\ p_{1n}(\bar{i}) \end{bmatrix}^T, \quad (102)$$

together with the equality

$$Q_{I,\bar{i}} Q_{\bar{i}\bar{i}}^{-1} \bar{i} = \hat{\mathbb{I}} - \hat{\mathbb{I}} \quad (103)$$

\square

Proof of Theorem 3 We apply the least-squares conditional adjustment to the GF ambiguity-float network correction (51). Given the extra redundancy by the geometry-based network model (Table 6), the following sets of misclosures are formed

$$t_g = (I_{n-1} \otimes (D_m^T G)^{\perp T}) [\hat{\rho}_{12}^T(\bar{i}), \dots, \hat{\rho}_{1n}^T(\bar{i})]^T, \\ t_{g_{ll}} = (I_{k-1} \otimes D_m^T) [\hat{\rho}_{1l}^T(12), \dots, \hat{\rho}_{1l}^T(1k)]^T \quad (104)$$

$l = 2, \dots, n$. The first set of misclosures t_g is due to the ‘geometry-parametrization’ of (72). The $(n-1)$ sets of misclosures $t_{g_{ll}}$ are due to the fact that the relative position increments and ZTDs ($\Delta x_l - \Delta x_1$) are assumed *constant* over k epochs. According to the least-squares conditional adjustment, the GB ambiguity-float network correction (75) is obtained as

$$\begin{bmatrix} \hat{\tilde{c}}_{\phi, GB}(i) \\ \hat{\tilde{c}}_{p, GB}(i) \end{bmatrix} = y - Q_{y,t_g} Q_{t_g t_g}^{-1} t_g - Q_{y,t_{g_L}} Q_{t_{g_L} t_{g_L}}^{-1} t_{g_L} \quad (105)$$

with $y = [\hat{\tilde{c}}_{\phi, GF}^T(i), \hat{\tilde{c}}_{p, GF}^T(i)]^T$ and $t_{g_L} = [t_{g_{12}}^T, \dots, t_{g_{1n}}^T]^T$. Equation (75) follows then by substituting

$$Q_{y,t_g} Q_{t_g t_g}^{-1} t_g = \hat{V}, \quad \text{and} \quad Q_{y,t_{g_L}} Q_{t_{g_L} t_{g_L}}^{-1} t_{g_L} = \hat{V} \quad (106)$$

into (105). \square

Proof of Theorem 4 We apply the least-squares conditional adjustment to the GF ambiguity-fixed network correction (57), on the basis of the extra geometry-based misclosures given in (104). The GB ambiguity-fixed network correction (81) follows then through replacing the role of y in (105) by $\tilde{y} = [\hat{\tilde{c}}_{\phi, GF}^T(i), \hat{\tilde{c}}_{p, GF}^T(i)]^T$, together with the equalities

$$Q_{\tilde{y}, t_g} Q_{t_g t_g}^{-1} t_g = \tilde{V}, \quad \text{and} \quad Q_{\tilde{y}, t_{g_L}} Q_{t_{g_L} t_{g_L}}^{-1} t_{g_L} = \tilde{V} \quad (107)$$

\square

References

- Baarda W (1973) S-transformations and Criterion Matrices. Tech. rep., Netherlands Geodetic Commission, Publ. on Geodesy, New Series, Vol. 5(1), Delft
- Banville S, Collins P, Zhang W, Langley RB (2014) Global and Regional Ionospheric Corrections for Faster PPP Convergence. *Navigation* 61(2):115–124
- Bertiger W, Desai SD, Haines B, Harvey N, Moore AW, Owen S, Weiss JP (2010) Single receiver phase ambiguity resolution with GPS data. *J Geod* 84(5):327–337
- Blewitt G (1989) Carrier phase ambiguity resolution for the Global Positioning System applied to geodetic baselines up to 2000 km. *J Geophys Res* 94(B8)
- Collins P (2008) Isolating and estimating undifferenced GPS integer ambiguities. In: Proc. ION NTM, pp 720–732
- Ge M, Gendt G, Rothacher M, Shi C, Liu J (2008) Resolution of GPS carrier-phase ambiguities in precise point positioning (PPP) with daily observations. *J Geod* 82(7):389–399
- Geng J, Bock Y (2013) Triple-frequency GPS precise point positioning with rapid ambiguity resolution. *J Geod* 87(5):449–460
- Geng J, Shi C, Ge M, Dodson AH, Lou Y, Zhao Q, Liu J (2012) Improving the estimation of fractional-cycle biases for ambiguity resolution in precise point positioning. *J Geod* 86(8):579–589
- Grejner-Brzezinska DA, Wielgosz P, Kashani I, Smith DA, Spencer PS, Robertson DS, Mader GL, et al (2004) An analysis of the effects of different network-based ionosphere estimation models on rover positioning accuracy. *J GPS* 3(1-2):115–131
- Grejner-Brzezinska DA, Kashani I, Wielgosz P, Smith DA, Spencer PS, Robertson DS, Mader GL (2007) Efficiency and reliability of ambiguity resolution in network-based real-time kinematic GPS. *J Surv Eng* 133(2):56–65
- Henderson HV, Pukelsheim F, Searle SR (1983) On the History of the Kronecker Product. *Linear and Multilinear Algebra* 14(2):113–120
- Heroux P, Kouba J (1995) GPS precise point positioning with a difference. In: Paper presented at Geomatics 95, Ottawa, Ontario, Canada, 13-15 June
- Hofmann-Wellenhof B, Lichtenegger H, Wasle E (2008) GNSS: Global Navigation Satellite Systems: GPS, Glonass, Galileo, and More. Springer, New York
- Jonkman N, Teunissen P, Joosten P, Odijk D (2000) GNSS long baseline ambiguity resolution: impact of a third navigation frequency. In: Geodesy Beyond 2000, IAG Symp 121, pp 349–354
- Lannes A, Prieur JL (2013) Calibration of the clock-phase biases of GNSS networks: the closure-ambiguity approach. *J Geod* 87(8):709–731
- Lannes A, Teunissen PJG (2011) GNSS algebraic structures. *J Geod* 85(5):273–290
- Laurichesse D, Mercier F (2007) Integer ambiguity resolution on undifferenced GPS phase measurements and its application to PPP. In: Proceedings of the 20th International Technical Meeting of the Satellite Division of The Institute of Navigation (ION GNSS 2007), pp 839–848
- Li B, Shen Y, Feng Y, Gao W, Yang L (2014) GNSS ambiguity resolution with controllable failure rate for long baseline network RTK. *J Geod* 88(2):99–112
- Li X, Zhang X (2012) Improving the estimation of uncalibrated fractional phase offsets for PPP ambiguity resolution. *Journal of Navigation* 65(03):513–529
- Li X, Ge M, Zhang H, Wickert J (2013) A method for improving uncalibrated phase delay estimation and ambiguity-fixing in real-time precise point positioning. *J Geod* 87(5):405–416
- Loyer S, Perosanz F, Mercier F, Capdeville H, Marty JC (2012) Zero-difference GPS ambiguity resolution at CNES–CLS IGS

- Analysis Center. *J Geod* 86(11):991–1003
- Mervart L, Lukes Z, Rocken C, Iwabuchi T (2008) Precise Point Positioning with ambiguity resolution in real-time. In: Proceedings of ION GNSS, pp 397–405
- Mervart L, Rocken C, Iwabuchi T, Lukes Z, Kanzaki M (2013) Precise Point Positioning with Fast Ambiguity Resolution—Prerequisites, Algorithms and Performance. In: Proceedings of ION GNSS, pp 1176–1185
- Odijk D (2002) Fast precise GPS positioning in the presence of ionospheric delays. Ph.D. thesis, Delft University of Technology, Publication on Geodesy, 52, Netherlands, Geodetic Commission, Delft
- Odijk D, Teunissen PJG (2008) ADOP in closed form for a hierarchy of multi-frequency single-baseline GNSS models. *J Geod* 82(8):473–492
- Odijk D, Teunissen PJG, Zhang B (2012) Single-frequency integer ambiguity resolution enabled GPS precise point positioning. *J Surv Eng* 138(4):193–202
- Odijk D, Arora BS, Teunissen PJG (2014) Predicting the success rate of long-baseline GPS+Galileo (partial) ambiguity resolution. *The Journal of Navigation* 67(3):385–401
- Schaer S (1999) Mapping and predicting the Earth's ionosphere using the Global Positioning System. PhD thesis, University of Bern, Bern, Switzerland
- Teunissen P, Jonkman N, Joosten P, Tiberius C (2000) Long baseline 3 frequency differential GNSS. In: Position Location and Navigation Symposium, IEEE 2000, San Diego, CA, pp 7–14, DOI 10.1109/PLANS.2000.838277
- Teunissen PJG (1985) Generalized inverses, adjustment, the datum problem and S-transformations. In: Optimization and Design of Geodetic Networks, EW Grafarend and F Sanso (Eds), Springer
- Teunissen PJG (1997a) A canonical theory for short GPS baselines. Part I: The baseline precision. *J Geod* 71(6):320–336
- Teunissen PJG (1997b) A canonical theory for short GPS baselines. Part IV: Precision versus reliability. *J Geod* 71(9):513–525
- Teunissen PJG (2000) Adjustment Theory: an Introduction. Delft University Press, series on Mathematical Geodesy and Positioning
- Teunissen PJG, Khodabandeh A (2014) Do GNSS parameters always benefit from integer ambiguity resolution? a PPP-RTK network scenario. In: Proceedings of ION GNSS+, Tampa, Florida, pp 590–600
- Teunissen PJG, Khodabandeh A (2015) Review and Principles of PPP-RTK methods. *J Geod* 89(3):217–240
- Teunissen PJG, Kleusberg A (1998) GPS for Geodesy, 2nd edn. Springer Berlin
- Teunissen PJG, Odijk D, Zhang B (2010) PPP-RTK: Results of CORS Network-Based PPP with Integer Ambiguity Resolution. *J Aeronaut, Astronaut Aviat* 42(4):223–229
- Verhagen S (2002) Studying the Performance of Global Navigation Satellite Systems: a New Software Tool. *GPS world* 13(6):60–65
- Wielgosz P, Krankowski A, Sieradzki R, Grejner-Brzezinska DA (2008) Application of predictive regional ionosphere model to medium range RTK positioning. *Acta Geophysica* 56(4):1147–1161
- Wubbena G, Schmitz M, Bagg A (2005) PPP-RTK: Precise Point Positioning using state-space representation in RTK networks. In: Proceedings of ION GNSS, pp 13–16
- Yu X, Zhang X, Liu J, Shi J, Cai C, Gao Y (2011) Performance Assessment of Long-baseline Integer Ambiguity Resolution with Different Observation Models. In: Proceedings of ION GNSS, Portland OR, pp 688–698
- Zhang B, Teunissen PJG, Odijk D (2011) A novel un-differenced PPP-RTK concept. *J Navig* 64(S1):S180–S191
- Zhang X, Li P, Guo F (2013) Ambiguity resolution in precise point positioning with hourly data for global single receiver. *Adv Space Res* 51(1):153 – 161
- Zumberge JF, Heflin MB, Jefferson DC, Watkins MM, Webb FH (1997) Precise point positioning for the efficient and robust analysis of GPS data from large networks. *J Geophys Res* 102:5005–5017